Dinuclear Rare-Earth β-Diketiminates with Bridging 3,5-Di*tert*-butyl-catecholates: Synthesis, Structure, and Single-Molecule Magnet Properties

Svetlana V. Klementyeva,* Michael T. Gamer, Michael Schulze, Nithin Suryadevara, Artem S. Bogomyakov, Pavel A. Abramov, Sergey N. Konchenko, Mario Ruben,* Wolfgang Wernsdorfer,* and Eufemio Moreno-Pineda*

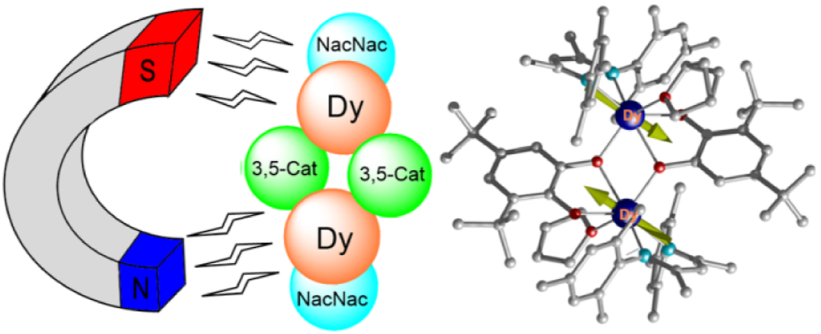

ABSTRACT: The dinuclear β-diketiminato complex $[L^1ClDy(\mu\text{-}Cl)_3DyL^1(THF)]$ (**1**) (L^1 = {2,6-^{i}Pr$_2$C$_6$H$_3$–NC(Me)CHC(Me)-N-2,6-^{i}Pr$_2$C$_6$H$_3$}$^-$) was obtained by reaction of $DyCl_3$ with KL^1 in a molar ratio of 1:1 and used for the preparation of the mixed-ligand complex $[L^1Dy(\mu\text{-}3,5\text{-}Cat)]_2$ (**2**) by salt metathesis reaction with 3,5-CatK_2 (3,5-Cat −3,5-di-*tert*-butyl-catecholate). Reactions of 3,5-CatNa_2 with $[L^2LnCl_2(THF)_2]$ (Ln^{3+} = Dy, Y) ligated with the less bulky ligand L^2 = {2,4,6-Me$_3$C$_6$H$_2$–NC(Me)CHC(Me)N-2,4,6-Me$_3$C$_6$H$_2$}$^-$ afforded the mixed-ligand THF-containing complexes $[L^2Ln(\mu\text{-}3,5\text{-}Cat)(THF)]_2$ (Ln^{3+} = Dy (**3a**), Y (**3b**)). All new complexes were fully characterized, and the solid-state structures were determined by single-crystal X-ray diffraction. Magnetic measurements revealed single-molecule magnet behavior for the dysprosium complexes. Sub-Kelvin μSQUID studies confirm the SMM character of the systems, while CASSCF calculation along with simulation of the experimental data yields an antiferromagnetic interaction operating between the Dy^{3+} ions.

INTRODUCTION

Mixed-ligand complexes attract considerable attention due to the combination of several structural and chemical features providing a useful variation of ligand characteristics and mutual influence on the metal center and the coordination environment. *N*-Aryl-substituted β-diketiminates or "NacNac" ancillary ligands {ArNC(R)CHC(R)NAr}$^-$ are well-established ligands supporting rare-earth metals.[1−6] The bulkiness of these ligands combined with easily tunable steric and electronic properties at the nitrogen atoms and the carbon backbone substituents, in combination with the formation of six-membered chelating rings, provides a wide application in coordination and organometallic chemistry. The utilization of β-diketiminates in organolanthanide chemistry is of substantial current interest because they allow the isolation of low-coordinate metal complexes showing unique bonding[2] or unusual reactivity.[3−5] Besides the classical role of spectator ligands, β-diketiminates behave as noninnocent ligands and may be involved in different transformations including redox reactions and metal−ligand cooperative activation of substrates.[6]

Surprisingly, only a few rare-earth metal complexes coordinated by *o*-quinonato ligands are known.[7−10] Recently, dinuclear $[(Ln^{III}Cp^*)_2(3,6\text{-}Cat)_2]$ (Ln^{III} = Sm, Yb; Cp* = η^5-C_5Me_5) and trinuclear $[(Eu^{III}Cp^*)(Eu^{II}\cdot THF)_2(3,6\text{-}Cat)_3]$ mixed-ligand complexes with bridging 3,6-di-*tert*-butyl-catecholates (3,6-Cat) have been prepared by the reduction of 3,6-di-*tert*-butyl-*o*-quinone (3,6-DTBQ) with lanthanocenes $Cp^*_2Ln^{II}(THF)_2$ (Ln^{II} = Sm, Yb, Eu).[7a] In addition, a reduction of 9,10-phenanthrenequinone with samarocene to

Scheme 1. Synthesis of Complex 1

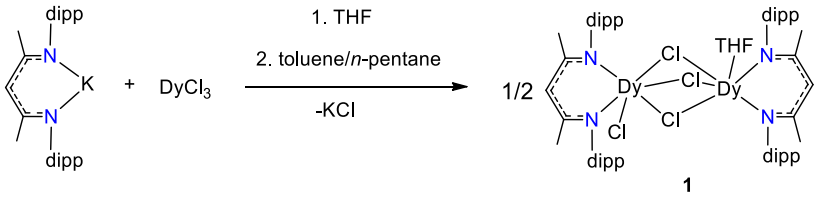

1

Scheme 2. Synthesis of Complexes 2 and 3a,b

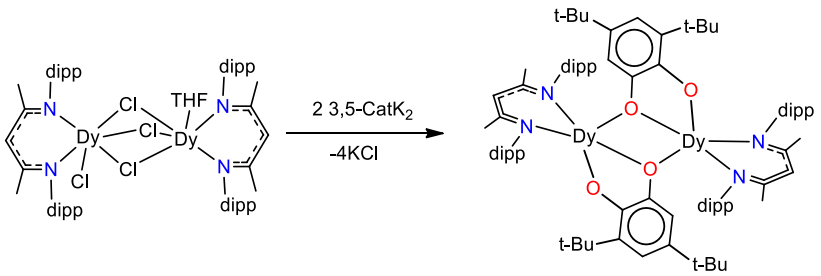

2

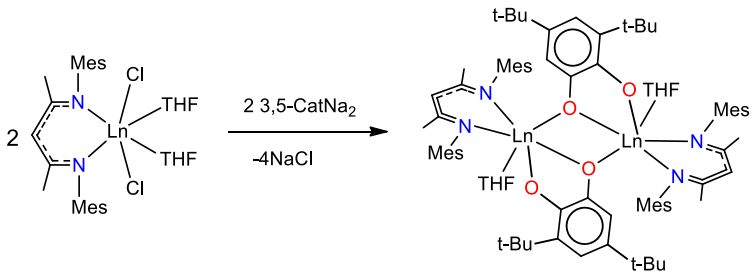

Ln = Dy (**3a**), Y (**3b**)

give a series of polynuclear samarocene complexes has been studied.[7b] Synthesis and crystal structure of some yttrium complexes with 3,6-Cat have been also reported.[8] Single-molecular magnet behavior of the dinuclear dysprosium complex $[Dy_2(hfac)_6(H_2O)_2(Q\text{-}TTF\text{-}Q)]$ (hfac = 1,1,1,5,5,5-hexafluoroacetylacetonate, Q-TTF-Q = 4,4′,7,7′-tetra-*tert*-butyl-2,2′-bi-1,3-benzodithiole-5,5′,6,6′-tetraone) was found[9a] among a series of rare-earth element derivatives of such redox-active triad *o*-quinone−tetrathiafulvalene−*o*-quinone in the neutral form of the ligand.[9] Sterically hindered 3,5-di-*tert*-butyl-*o*-quinone (3,5-DTBQ) was also involved in the lanthanide chemistry.[10] Magnetic properties of some mixed-ligand 3,5-di-*tert*-butyl-*o*-semiquinonate lanthanide derivatives coordinated by hydrotris(pyrazolyl)borate were investigated in detail.[11]

First of all, dysprosium derivatives have attracted unabated attention due to their magnetic properties. Dy^{3+} ion with an odd number of f-electrons, a large magnetic moment and high magnetic anisotropy of the 4f shell combined with a large energy gap between the ground and first excited states, as well as strong axial ligand field, is considered to be an ideal ion for Dy-SMMs; thus, the number of dysprosium-based SMMs increases steadily.[12] For the magnetic properties of lanthanide compounds, the geometry of the coordination sphere plays a crucial role. Therefore, the search for new ligand systems for creating complexes of rare-earth metals with interesting magnetic properties has boosted the research activity in this field. In recent years, appreciable progress in the study of lanthanide SMMs has been achieved and new records for the relaxation energy barrier and the blocking temperature have been established.[13] However, one of the stumbling blocks in developing SMMs with a high-energy barrier is the zero-field quantum tunneling of magnetization (QTM) through the degenerated ground states. Different strategies have been successfully exploited to suppress QTM and thus enhance the SMM properties.[14] One of them is based on the magnetic coupling between lanthanide ions, for example, in the dinuclear lanthanide compounds.[15] It has been shown that bridging ligands with diffuse spin orbitals (especially radicals[16] or heavy main group elements[17]) provide an effective suppression of QTM. A number of different bridging ligands such as N-oxides,[18] Schiff bases,[19] phenoxides,[20] hydroxides,[21] and arenes[22] have been used for construction of dinuclear motifs in the lanthanide-based SMMs. The utilization of redox ligands in lanthanide compounds is also considered to be a prospective approach for elaborating SMMs.[23] A particular example of such redox-active ligands is bridging *o*-quinonato ligands, which also support the SMM behavior of lanthanide compounds.[24]

Recently, we have reported a convenient synthetic route for the preparation of mononuclear dichlorides of trivalent rare earths ligated by mesityl-substituted *β*-diketiminate $[L^2LnCl_2(THF)_2]$ (Ln^{3+} = Y, Dy, Er)[25] and used them as starting materials for several mixed-ligand complexes.[26] These results encouraged us to synthesize 3,5-di-*tert*-butyl-catecholato (3,5-Cat) complexes of some rare earth in combination with different *β*-diketiminates. In order to compare the influence of the different steric demands of the ligands on the coordination environment of the rare-earth elements in the target

complexes, two types of bulky *N*-aryl-substituted β-diketiminates with 2,6-diisopropylphenyl (L^1 = {2,6-^{i}Pr$_2$C$_6$H$_3$−NC(Me)CHC(Me)N-2,6-^{i}Pr$_2$C$_6$H$_3$}$^-$) and mesityl (L^2 = {2,4,6-Me$_3$C$_6$H$_2$−NC(Me)CHC(Me)N-2,4,6-Me$_3$C$_6$H$_2$}$^-$) substituents have been studied. Presumably, the steric stabilization imparted by such bulky groups allows for the preparation of low-coordinated complexes. Continuing our study on mixed-ligand rare-earth complexes coordinated by β-diketiminate spectator ligands, we report herein the synthesis, molecular structures, as well as magnetic properties of a series of dinuclear lanthanide derivatives with bridging catecholates.

RESULTS AND DISCUSSION

Synthesis. Reaction of KL^1 with anhydrous $DyCl_3$ (Scheme 1) in a 1:1 molar ratio in refluxing THF followed by heating in toluene at 90 °C led to the pale-yellow-green-colored solution and precipitation of KCl. The subsequent workup allows for the isolation of the dinuclear complex [L^1ClDy(μ-Cl)$_3$DyL^1(THF)] (**1**) as an analytically pure crystalline solid in good yield. The composition of compound **1** was determined by elemental analysis. Moreover, strong absorption near 1550 and 1525 cm^{-1} in the IR spectrum (Figure S1) indicates a coordination of the β-diketiminato ligand.[1−5,25−27] Complex **1** is sensitive to atmospheric moisture due to easy hydrolysis of the β-diketiminate ligand and is long stable only in an inert atmosphere.

Salt metathesis of lanthanide halides supported by β-diketiminates has been proven to be a very fruitful synthetic approach to mixed-ligand compounds.[5,26,27] To continue these studies, we performed some reactions of two types of sterically hindered β-diketiminates with alkali metal salts of 3,5-Cat. The salt metathesis of β-diketiminate-decorated dysprosium chloride **1** with potassium 3,5-di-*tert*-butyl-catecholate (3,5-CatK_2) in THF at room temperature afforded the dimeric nonsolvated complex [L^1Dy(μ-3,5-Cat)]$_2$ (**2**) (Scheme 2). After evaporation of THF, the remaining residue was doubly treated with *n*-hexane followed by slow extraction with *n*-hexane yielding single crystals of **2** suitable for single-crystal X-ray diffraction.

The dimeric mixed-ligand complexes of the mesityl-substituted β-diketiminate ligand [L^2Ln(μ-3,5-Cat)(THF)]$_2$ (Ln^{3+} = Dy (**3a**), Y (**3b**)) were obtained under similar conditions from [L^2LnCl$_2$(THF)$_2$] (Ln^{3+} = Dy, Y)[25] and sodium 3,5-di-*tert*-butyl-catecholate in THF (Scheme 2). Single crystals are readily formed by slow evaporation of THF. The dinuclear mixed-ligand compounds **3a,b** are insoluble in most organic solvents; therefore, NMR spectra of yttrium compounds were not recorded. Their composition was determined by single-crystal X-ray diffraction, IR spectroscopy (Figures S2 and S4), and elemental analysis. The IR spectra exhibited stretching vibrations of the β-diketiminato ligands near 1550 and 1525 cm^{-1}.[1−6,25−27] The bands at ca. 1255 cm^{-1} are typical for stretching vibrations of the C−O bonds in catecholates.[28] The mixed-ligand complexes **2** and **3a,b** are extremely air sensitive because of the presence of easily oxidizable redox-active catecholates and long stable only in an inert atmosphere.

The described subsequent salt metathesis reactions (Schemes 1 and 2) are considered to be a very prospective method for accessing the desired mixed-ligand complexes containing sterically hindered β-diketiminato ligands and redox-active ligands, which are able to be reduced to the dianionic form.

Single-Crystal X-ray Diffraction Studies. Single crystals of **1** suitable for X-ray diffraction were obtained by layering a toluene solution carefully with *n*-pentane and subsequent storage of this mixture for 3 weeks at ambient temperature. Complex **1** is entirely isostructural with the analogous erbium complex[27a] and somewhat differs from the samarium,[27b] ytterbium,[27c] and yttrium[27d] compounds. A detailed description of the molecular structure of **1** is given in the Supporting Information. Noteworthily, the coordination mode of 2,6-diisopropylphenyl-substituted β-diketiminato ligands is very typical for lanthanide compounds with a common formula, NacNacLnR$_2$.[4,5,25−27,29]

Similar to **1**, complex **2** crystallizes in the monoclinic $P2_1/n$ space group, with four molecules in the asymmetric unit. The molecular structure of complex **2** is shown in Figure 1 and

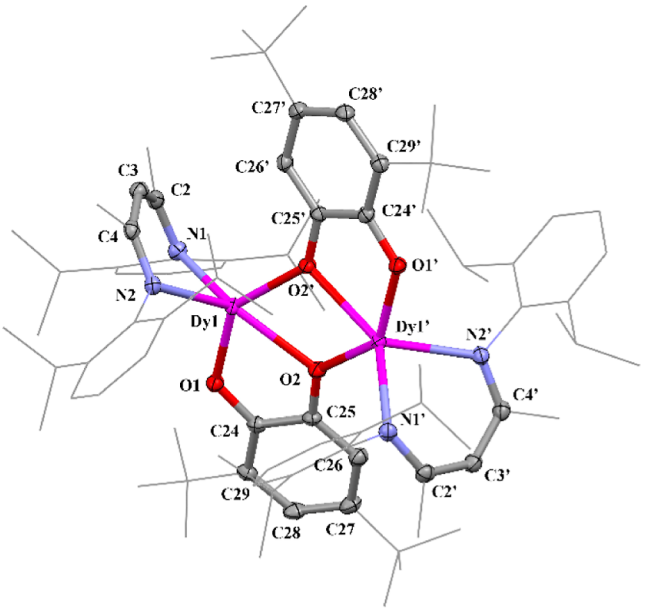

Figure 1. Molecular structure of **2**, omitting hydrogen atoms. Thermal ellipsoids are drawn at 50% probability.

reveals some differences in comparison with the similar yttrium compound [L^1Y(μ-3,5-Cat)]$_2$ state reported earlier.[26c] The yttrium analogue has a centrosymmetrically dimeric structure in the solid, while dysprosium complex **2** has an inversion center in the middle of the central Ln-O2-Ln′-O2′ ring.

The coordination mode of the 2,6-diisopropylphenyl-substituted β-diketiminato ligands, with slight asymmetric Ln−N bonds and acute N−Ln−N angles as well as with the nearly perpendicular orientation of the arene rings to the N−C−C−N backbone plane, is quite similar to that found in chlorides described above and complexes published earlier.[4,5,25−27,29] In complex **2**, the deviation of both dysprosium atoms from the planes of the N−C−C−N ligand backbone is more than 1 Å (1.114 Å for Dy1 and 1.002 Å for Dy1′), while the both central carbon atoms (C3 and C3′) deviate from the corresponding planes of β-diketiminato ligands by 0.111 Å. These parameters are comparable to those found in the corresponding dinuclear chloride **1** and its analogues.[27] Due to the asymmetry of **2**, both β-diketiminato ligands are not parallel to each other. The corresponding dihedral angle between the planes of the N−C−C−N backbone is 42.16°.

Compounds **3a,b** supported by mesityl-substituted β-diketiminato ligands are isostructural and crystallize in triclinic space group $P\bar{1}$ with one molecule in the unit cell. As an example, dysprosium compound **3a** is depicted in Figure 2.

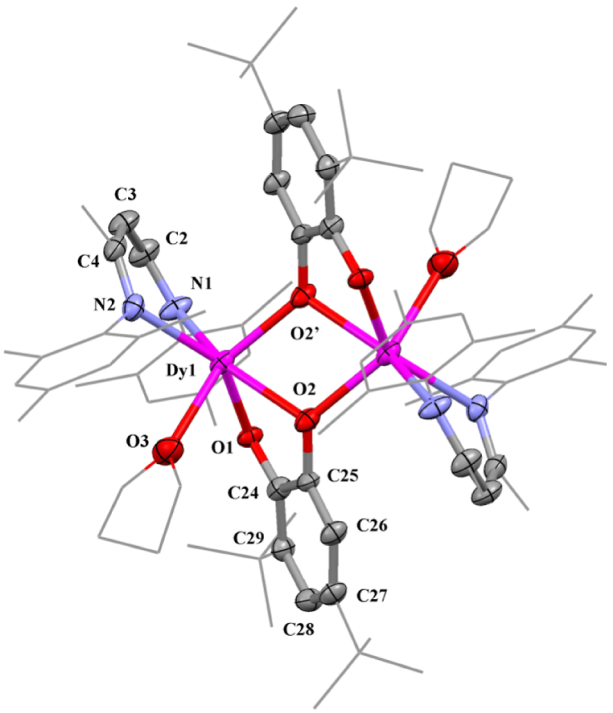

Figure 2. Molecular structure of **3a**, omitting hydrogen atoms. Thermal ellipsoids are drawn at 50% probability.

Noteworthily, the crystallization of compounds **3a,b**, under the conditions described for **2**, led to another polymorph crystallizing in the monoclinic space group *C2c* with a small difference in the ligand conformation (see, for example, the molecular structure of **3a′** in the Supporting Information (Figure S6)).

Six-membered chelating rings formed by mesityl-decorated β-diketiminato ligands have a typical structure with slight asymmetric Ln−N bonds and acute N−Ln−N angles (Table 1).[4,5,25−27,29] The rare-earth atoms deviate from the N−C−C−N backbone plane by 0.878 Å (**3a**) and 0.671 Å (**3b**), while the central carbon atoms occupy the usual positions with the corresponding deviation of 0.118 Å (**3a**) and 0.159 Å (**3b**) from the N−C−C−N plane. The arene rings are nearly perpendicularly oriented to the NCCN backbone plane in all cases (see Table 2).

Interestingly, each catecholate acts in compounds **2** and **3a,b** as a bridging ligand, with one oxygen atom coordinating in a μ-mode. Consequently, the corresponding C25−O2 bond is significantly elongated in comparison with the nonbridging C24−O1 bond (Figures 1 and 2) and the C−O bonds in different catecholate complexes.[28] Moreover, the Ln−O bond lengths of the μ-oxygen atoms are 0.1−0.15 Å longer than the terminal Ln−O bonds. The bridging character of these ligands causes unusual bond length alternation in catecholate rings. The evident distortion of the catecholate rings from the planar structure, especially in the complexes supported by mesityl-substituted β-diketiminate (**3a,b**), results from the complexes' steric strain.

The most evident difference in the structures of complexes **2** and **3a** is the polyhedral shape of the Dy^{3+} centers. According to the polyhedral shape analysis with SHAPE 2.1[30] (for details, see the Supporting Information), the first coordination sphere of Dy atoms in **2** is close to a distorted square pyramidal geometry, while in **3a**, it adopts a trigonal prism geometry (Figure 3).

Both Dy^{3+} ions in **2** are 5-fold coordinated, forming a distorted tetragonal pyramidal geometry. The β-diketiminato ligand coordinates as a bidentate ligand in a chelating mode. Both bridging oxygen atoms O2 and O2′ and the nonbridging one, O1, as well as nitrogen atom N1 form the basal plane, while the other nitrogen atom N2 of β-diketiminate occupies

Table 1. Selected Bond Lengths (Å) and Angles (°) for Complexes 2 and 3a,b

	2		3a	3b
Ln1−O2′	2.2606(16)	2.2515(17)[a]	2.232(3)	2.225(3)
Ln1−O3			2.420(4)	2.344(7)
Ln1−N1	2.3207(19)	2.3675(18)	2.395(4)	2.365(14)
Ln1−N2	2.3573(18)	2.3248(19)	2.389(4)	2.338(18)
Ln1−O1	2.1122(15)	2.1120(15)	2.178(3)	2.178(2)
Ln1−O2	2.3823(15)	2.3944(15)	2.329(3)	2.3213(19)
N1−C2	1.337(3)	1.334(3)	1.330(6)	1.321(18)
C2−C3	1.399(3)	1.411(3)	1.392(7)	1.401(13)
C3−C4	1.412(3)	1.398(3)	1.405(7)	1.381(14)
N2−C4	1.329(3)	1.340(3)	1.337(6)	1.37(3)
O1−C24	1.352(3)	1.352(2)	1.347(5)	1.348(3)
O2−C25	1.381(2)	1.382(2)	1.390(6)	1.390(4)
C24−C25	1.404(3)	1.403(3)	1.404(7)	1.402(4)
C25−C26	1.390(3)	1.390(3)	1.393(6)	1.384(4)
C26−C27	1.400(3)	1.399(3)	1.371(6)	1.392(5)
C27−C28	1.395(3)	1.393(3)	1.384(7)	1.382(4)
C28−C29	1.394(3)	1.396(3)	1.409(6)	1.399(4)
C24−C29	1.407(3)	1.409(3)	1.390(7)	1.416(4)
N1−Ln1−N2	83.01(6)	81.56(7)	77.71(14)	79.0(6)

[a]The values in this column correspond to the half of the molecule of **2** with the symbols Dy1′, *N*′, O′, and C′.

Table 2. Crystallographic Data and Selected Refinement Details for Complexes 1, 2, and 3a,b

	2	3a	3b
empirical formula	$C_{86}H_{122}Dy_2N_4O_4$	$C_{82}H_{114}N_4O_6Dy_2$	$C_{82}H_{114}N_4O_6Y_2$
formula weight	1600.87	1576.77	1429.59
temperature (K)	150	150	100
crystal size (mm3)	0.25 × 0.22 × 0.12	0.217 × 0.124 × 0.042	0.121 × 0.089 × 0.049
crystal system	monoclinic	triclinic	triclinic
space group	$P2_1/n$	$P\bar{1}$	$P\bar{1}$
Z	4	1	1
a (Å)	13.902 (3)	13.429(2)	13.4329(6)
b (Å)	41.933 (8)	13.724(2)	13.7000(6)
c (Å)	14.163 (3)	13.898(3)	13.8906(8)
α (deg)	90	64.016(13)	63.661(4)
β (deg)	103.35 (3)	72.092(14)	71.577(4)
γ (deg)	90	71.017(13)	70.752(3)
V (Å^3)	8033 (3)	2135.8(7)	2118.9(2)
$D_{calcd.}$ (g cm^{-3})	1.324	1.226	1.120
μ (Mo K_α) (mm^{-1})	1.90	1.783	1.411
θ range (deg)	3.3−31.2	1.63−29.24	1.70−31.48
h, k, and l index range	$-19 \le h \le 19$,$-60 \le k \le 58$,$-19 \le l \le 19$	$-16 \le h \le 15$; $-16 \le k \le 16$; $-17 \le l \le 17$	$-16 \le h \le 15$; $-16 \le k \le 16$; $-17 \le l \le 14$
F(000)	3320	814	760
reflections collected	84,064	19,614	19,840
unique reflections	20,835 (R_{int} = 0.023)	8378 (R_{int} = 0.1131)	8299 (R_{int} = 0.0793)
parameters refined	865	441	704
$R[F^2 > 2\sigma(F^2)]$	$R1$ = 0.0297 $wR2$ = 0.0586	$R1$ = 0.0410 $wR2$ = 0.0738	$R1$ = 0.0463 $wR2$ = 0.0788
$R(F^2)$ (all data)	$R1$ = 0.0363 $wR2$ = 0.0607	$R1$ = 0.0694 $wR2$ = 0.0846	$R1$ = 0.0965 $wR2$ = 0.0911
GOOF on F^2	1.146	0.878	0.875
$\Delta\rho_{max}$, $\Delta\rho_{min}$ (e Å^{-3})	1.72, −1.25	1.179, −0.800	0.411, −0.527

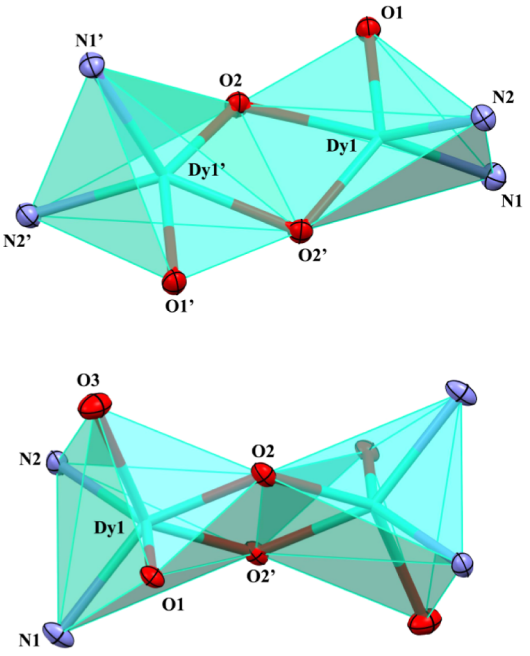

Figure 3. Polyhedral around Dy^{3+} centers in **2** (top) and **3a** (bottom).

the apical position of the exceedingly distorted tetragonal pyramid. In complex **2**, Dy1 and Dy1′ are bridged by two catecholato oxygen atoms (O2 and O2′), generating an unsymmetrical four-membered Dy_2O_2 core with Dy−O−Dy angles of 109.38(6)° and 108.64(6)° and Dy···Dy distance of 3.782(4) Å.

Compounds **3a,b** form a centrosymmetrically dimeric structure in the solid state with two bridging catecholate ligands between two rare-earth metal atoms. Each metal atom is in the center of a distorted trigonal prism. Thus, in comparison to **2**, the reduced steric hindrance of the β-diketiminate ligand causes an increase in the coordination number of rare-earth atoms from five to six. The two nitrogen atoms of the β-diketiminato ligand (N1 and N2) and one μ-oxygen atom of one of the catecholate ligands (O2′) form one triangular base of the trigonal prism. The oxygen atom of the coordinated THF molecule (O3) and both oxygen atoms of the other catecholate ligands (O1 and O2) occupy the other basal positions. The four-membered Dy_2O_2 core in **3a** is centrosymmetric, the angle Dy−O−Dy of 109.50(13)° is close to these of **2**, while the Dy···Dy distance is 3.725(4) Å, which is slightly shorter than those of **2**. For both complexes, the Dy−O bond lengths are in the range of 2.1120(15)−2.420(4) Å, and the Dy−N bond lengths range from 2.3207(19) to 2.395(4) Å.

The shortest intermolecular Dy···Dy distances between the adjacent dinuclear molecules for **2** and **3a** are 11.537(4) and 10.319(4) Å, respectively, suggesting that the intermolecular dipole−dipole interaction could be negligible compared to intramolecular interaction, while the short intramolecular Dy···Dy distances in **2** and **3a** (3.782(4) and 3.725(4) Å) can provide the potential interaction between Dy^{3+} ions.

Magnetism. The static magnetic characteristics of all complexes were investigated by employing restrained polycrystalline samples under an applied field of 1 kOe. The room temperature $\chi_M T$ value for all complexes was 27.73 and 27.82 cm^3·K/mol, for **2** and **3a**, respectively (Figure 4). In all cases, the room temperature $\chi_M T$ value was found to be close to the expected for the two uncoupled ions, (cf., 28.33 cm^3·K/mol for two Dy^{3+} with $^6H_{15/2}$ and $g_J = 4/3$). Upon cooling, the $\chi_M T(T)$ product remains reasonably constant down to ∼50 K, where it rapidly decreases to 8.92 and 9.82 cm^3 mol K^{-1} at 2 K for **2**

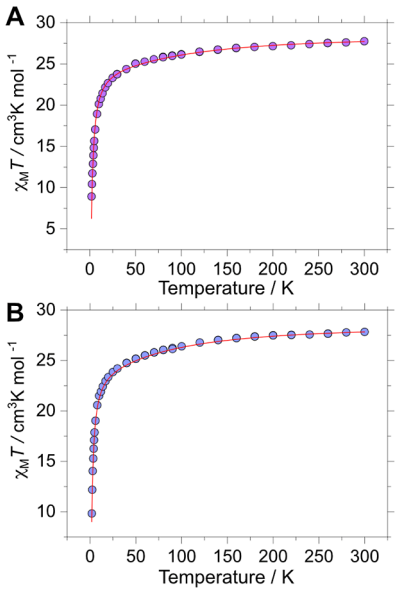

Figure 4. Static (DC) magnetic behavior under an applied DC field of 1 kOe: $\chi_M T$ data for **2** (**A**) and **3a** (**B**). The solid line is the fit employing the Lines model (eq 3) and the crystal field parameters as obtained from CASSCF.

and **3a**, respectively. The downturn observed for all sample signatures is crystal field effects and intramolecular magnetic interactions (vide infra). As a comparison, the $\chi_M T(T)$ for **1** has also been collected, leading to a similar profile to that of **2** and **3a**, with a downturn upon cooling appearing below 50 K (Figure S9).

The slow relaxing characteristics of lanthanide-based complexes make lanthanide-based complexes hot candidates for diverse technological applications.[31] Therefore, alternating current (AC) magnetic susceptibility studies probed the slow dynamic characteristics for all complexes and revealed a frequency-dependent magnetic susceptibility at zero field; hence, these are SMMs (Figure 5 and Figures S10–S15). For **1**, a maximum centered at 8 K is observed in the temperature dependence of the out-of-phase of the magnetic susceptibility ($\chi''(T)$) at the highest frequency (1512 Hz) (Figures S10–S11). The frequency-dependent magnetic susceptibility ($\chi''(\nu)$) reveals a maximum centered at 34 Hz at 2 K (Figure S11B). The maximum in $\chi''(\nu)$ remains practically constant upon increasing temperatures up to 4 K, where it becomes clearly temperature dependent, shifting to higher frequencies with increasing temperatures. In contrast, the maximum in the $\chi''(T)$ for **2** is observed at 13 K (1512 Hz), which shifts toward lower temperatures upon decreasing frequencies. The $\chi''(\nu)$ for **2** is centered at a lower frequency (8 Hz) at the lowest temperature (2 K) compared to **1** (cf. 34 Hz at 2 K), highlighting slower relaxation characteristics (Figure 5A,B). The maximum is affected slightly by the temperature increment up to 4 K, where it swiftly shifts toward higher frequencies. In stark contrast, the observed maximum in the $\chi''(T)$ for **3a** is observed at 23 K (1512 Hz). Moreover, in contrast to **1** and **2**, in which the $\chi''(\nu)$ maximum remains almost constant from 2 K up to 4 K, the $\chi''(\nu)$ maximum for **3a** lies below the experimental frequencies (at 2 Kp), with the maximum (0.1 Hz at 2 K) shifting swiftly upon temperature increment (Figure 5C,D). This behavior highlights slower relaxation characteristics for **3a** compared to those of **1** and **2**.

The relaxation times (τ) for **1**, **2**, and **3a** can be extracted from the magnetic susceptibility data by simultaneously fitting the $\chi'(\nu)$ and $\chi''(\nu)$ employing a generalized Debye model. The α parameters highlight a wide distribution of processes in all systems (Tables S4 and S5). The temperature dependence of the relaxation times $\tau(T)$ for **1** and **2** can be fitted employing the Raman and Orbach processes

$$\tau^{-1} = \tau_0^{-1}\exp(-U_{\text{eff}}/k_B T) + CT^n + \tau_{\text{QTM}}^{-1} \quad (1)$$

while the data for **1** can be fitted considering the Orbach and Raman processes leading to the following parameters $\tau_0 = 1.4(1) \times 10^{-5}$ s, $U_{\text{eff}} = 19.6(4)$ K (13.6(3) cm^{-1}), and $\tau_{\text{QTM}} = 4.4(1) \times 10^{-3}$ s (Figure S16A), while for **2**, the best fit yields $\tau_0 = 1.1(2) \times 10^{-6}$ s, $U_{\text{eff}} = 62(2)$ K (43(1) cm^{-1}), $C = 0.4(2)$ s^{-1}

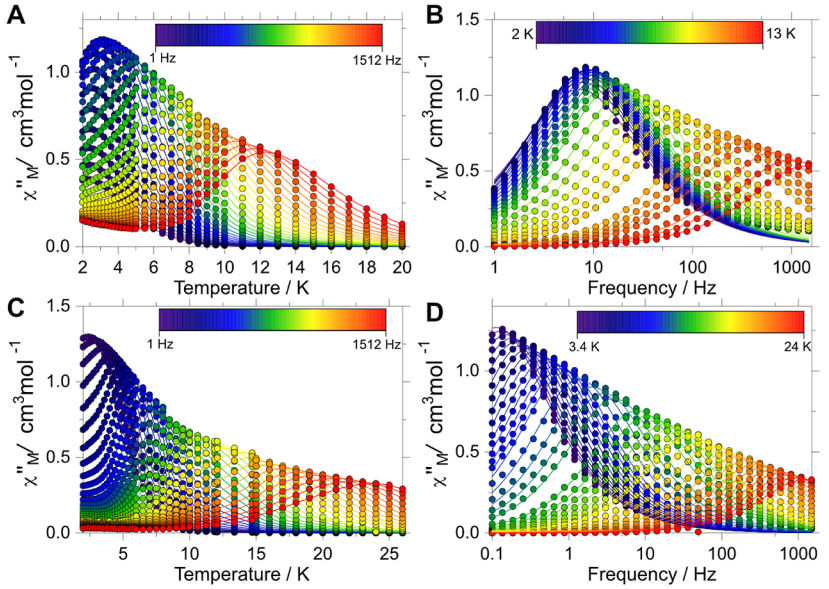

Figure 5. Dynamic studies: $\chi''(T)$ (left panels) and $\chi''(\nu)$ (right panels) for **2** (A,B) and **3a** (C,D) collected at zero applied DC field. Solid lines are the fit to a generalized Debye model.

K^{-n}, n = 3.2(4), and τ_{QTM} = 0.023(1) s (Figure S16B). For **3a**, solely the Raman process is sufficient to reproduce the $\tau(T)$ data with the best fit yielding $C = 9(1) \times 10^{-4}$ s^{-1} K^{-n}, n = 5.00(4) (Figure S16C). Notice that the Raman n parameters for **2** and **3a** are smaller than expected for Kramers ions.[32]

This can be caused by low vibration phonon-mediated relaxation.[33] To account for low phonon vibrations, the $\tau(T)$ was also fitted to

$$\tau^{-1} = \tau_0^{-1}\exp(-U_{eff}/k_BT) + \sum_{i=1}^{2} C_i \frac{\exp\left(\frac{\hbar\omega_i}{k_BT}\right)}{\left(\exp\left(\frac{\hbar\omega_i}{k_BT}\right) - 1\right)^2} + \tau_{QTM}^{-1} \quad (2)$$

where $\hbar\omega_i$ is the Raman vibrational modes and the last term accounts for the QTM process.[33b] Good fits are obtained with the inclusion of a single vibrational mode for **2**, yielding $\tau_0 = 2.8(5) \times 10^{-5}$ s, U_{eff} = 107(4) K (74(3) cm^{-1}), C_1 = 609(388) s^{-1}, $\hbar\omega_1$ = 9(2) cm^{-1}, and τ_{QTM} = 0.022(1) (Figure 6A). For

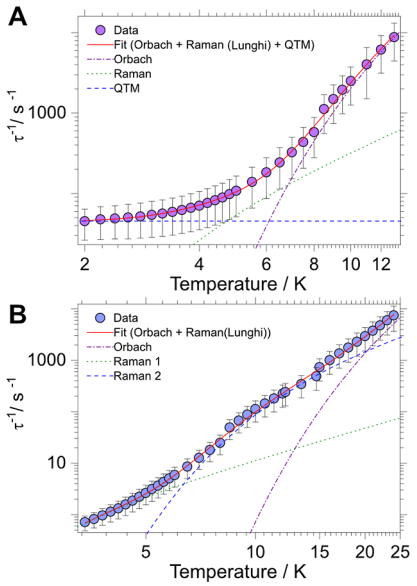

Figure 6. Relaxation characteristics: $\tau(T)$ profile and fits for **2** (A) and **3a** (B) employing eq 2 and parameters described in the text. The dotted/dashed lines are the contribution of each process to the overall fit (solid red line).

3a, two Raman vibrational modes were required without τ_{QTM} leading to $\tau_0 = 1(1) \times 10^{-5}$ s, U_{eff} = 283(43) K (197(30) cm^{-1}), C_1 = 13(6) s^{-1}, $\hbar\omega_1$ = 7(1) cm^{-1}, $C_2 = 1.9(4) \times 10^4$ s^{-1}, and $\hbar\omega_2$ = 37(2) cm^{-1}. As expected, the $\hbar\omega_i$ is low[33b,34] (Figure 7B).

***μ*SQUID.** Confirmation of the SMM characteristics of the complexes can be gained by studying the hysteretic behavior of the systems. For this, μSQUID loops were collected on single crystals of all complexes to confirm their SMM behavior. The μSQUID measurements were carried out on single crystals with the field applied along the easy axis of the crystal.[35] Hysteresis loop studies were performed at different sweeping rates, ranging from 0.5 to 128 mT/s, and temperatures from 5 to 30 mK (Figure 7). Open loops are found for all dysprosium complexes at the lowest temperature (Figure 7A,C), while the sweep-dependent loops highlight the expected behavior for the SMMs. The opening of the loops is only observable below 2 K. Moreover, the loops for **2** and **3a** showcase the characteristic S-shaped butterfly loops of antiferromagnetically coupled dimers.[34c,36] For **2**, a sharp tunneling event occurs at ±0.30 T, while a broader transition is also found at ±0.41 T (see Figure 9). Considering the dimeric nature of **2** and the fact that two differently oriented molecules reside in the unit cell, the two events correspond to the crossing between the antiferromagnetic ground state and the first excited coupled state. Note that the sharp crossing (±0.30 T) indicates that the applied field was close to the molecular easy axis of this molecule, while the broad transition and shifting to higher fields showcase a larger angle between the applied field and the molecular easy axes of the second molecule. A similar behavior is observed for **3a** with the crossing occurring at a smaller field ±0.22 T, denoting a smaller interaction between the Dy^{3+} ions. A single crossing was observed for **3a**, which can be ascribed to the sole presence of a single molecule residing in the unit cell. The inflection points observed in the μSQUID loops allow the determination of the mean exchange field (H_{ex}),[36a] leading to an effective exchange constant between the Ising spins of the Dy^{3+} ions: $H_{ex} = J_{ex}m_J/g_J\,\mu_B$, where m_J = 15/2 and g_J = 4/3. For **2**, J_{ex} = 36 mK (0.025 cm^{-1}) [for the ±0.30 T transition, closer to the easy axes] and for **3a**, J_{ex} = 26 mK (0.018 cm^{-1}). Note that the loops for **3a** have a larger opening between the near-zero field than that for **2**, which can be a consequence of pinning of a larger population of spins to the ferromagnetic excited state.

Open loops were also observed for **1**, with the narrowing of the opening upon warm up (Figure S17). However, two independent molecules are contained within the unit cell in **1**, and hence, the loops might be an average result of the magnetic anisotropy of the system and not the results of the single-molecular easy axes. Furthermore, it can be noted that the loops do not showcase the expected S-shaped butterfly loops characteristic of antiferromagnetically coupled Dy^{3+} dimers. This result indicates that the easy axes for the individual ions in **1** are not collinear.[37]

Theoretical Calculations. The magnetic characteristics of the dysprosium-based complexes can be understood through ab initio calculations, of the type CASSCF/SO-RASSI/SINGLE_ANISO approach implemented in the OpenMolcas.[38] For this purpose, the crystal structures of the complexes were employed without further optimizations (see the Supporting Information for details). The energies of low-lying Kramers doublets and the main components of the g tensor of the Dy^{3+} ions for **2** and **3a** are shown in Tables S6–S8. The ground Kramer doublet state characterizing both complexes is highly axial, with the g-values close to the expected values for a pure m_J = 15/2, i.e., g_z = 19.7 for **2** and g_z = 19.6 for **3a**. Likewise, the wave function composition of the ground state for these systems is highly pure (>95% m_J = ± 15/2). For **2**, two slightly different Dy^{3+} ions are found, as determined by the crystallographic studies, leading to faintly dissimilar characteristics (Tables S6–7). The first excited state is ca. 220 cm^{-1} from the ground doublet, while the second excited state lies at ca. 300 cm^{-1}. Similar characteristics are found for **3a**, with the first and second excited states at 202 and 327 cm^{-1}, respectively (Table S8). The main magnetic axes (z) for **2** and **3a** are depicted in Figure 8. CASSCF studies were also carried out for compound **1**. The obtained g-values are also axial, with similar separation (cf. 91 and 98 cm^{-1}) between the ground and first excited state (see Tables S9 and S10). In

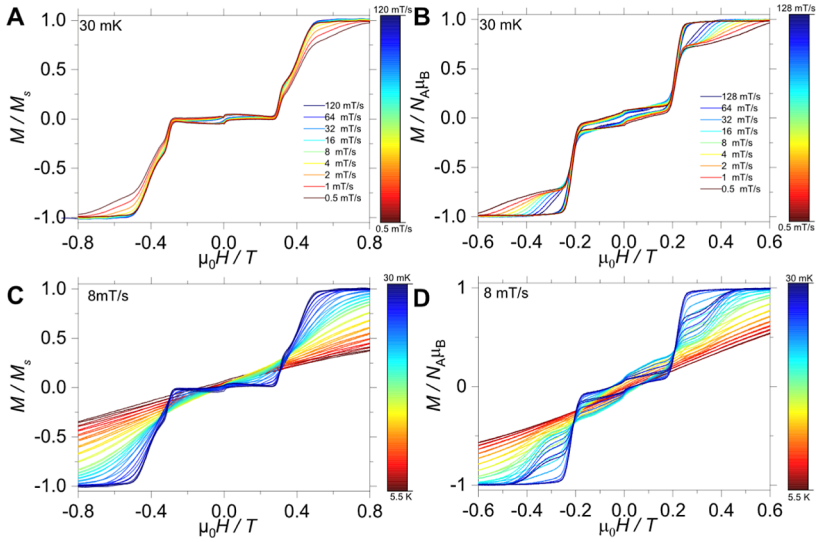

Figure 7. Sub-Kelvin μSQUID loops: temperature (A,B) and sweep-rate hysteresis loops for **2** (A,C) and **3a** (B,D).

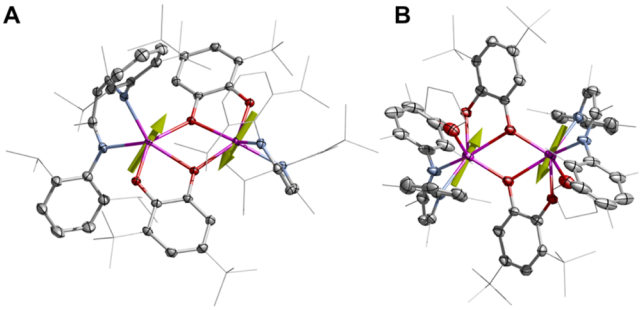

Figure 8. Molecular structure of **2** (A) and **3a** (B) with the main magnetic axis (green arrows).

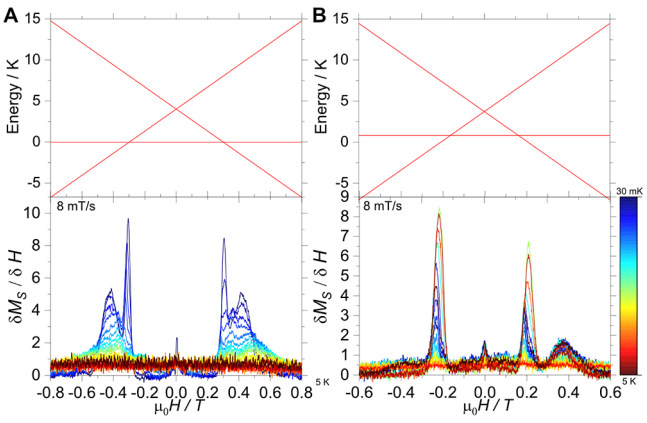

Figure 9. Energy diagram for **2** and **3a**: Zeeman diagram (top) and derivative of the field-sweep μSQUID loops (bottom) for **2** (A) and for **3a** (B). The broad transition centered to at +0.38 T corresponds to relaxation via the direct process.

contrast to **2** and **3a**, the anisotropy axes in **1** are not collinear, as a consequence of the asymmetry of the molecule (Figure S19), while the state composition of the ground doublet is less pure (>90% $m_J = \pm 15/2$) (Tables S9 and S10).

Although the CASSCF results pinpoint that the single-ion characteristics of **2** and **3a** are anisotropic, with a relatively large separation between the ground state and the first excited state, the magnetic characteristics must contemplate the presence of an interaction operating between the Dy^{3+} pairs. To this end, and with the knowledge of the crystal field parameters from CASSCF, it is possible to evaluate the interaction operating between the Dy^{3+} ions in **2** and **3a** employing the Lines model[39] by fitting the magnetic susceptibilities of the complexes.[40] The Lines model employs an isotropic exchange between the spin component of the angular momenta ($S = 5/2$ for Dy^{3+}) and the crystal field parameters obtained via CASSCF calculations. The Hamiltonian has the form

$$\mathcal{H}^{i}_{\mathrm{Dy}} = \mathcal{H}^{i}_{\mathrm{lf}} + g_J\mu_0\mu_B(\hat{J}_{\mathrm{Dy}(1)} + \hat{J}_{\mathrm{Dy}(2)})\boldsymbol{H}_z + \boldsymbol{J}^{i}_{\mathrm{Lines}}\hat{S}_{\mathrm{Dy}(1)}\hat{S}_{\mathrm{Dy}(2)} \quad (3)$$

where $\mathcal{H}^{i}_{\mathrm{lf}} = \sum_{k=2,4,6,-k\le q\le k} B^q_k O^q_k$ is the ligand field Hamiltonian expressed in the Steven's operator, O^q_k is the Stevens operator, and B^q_k is the ligand field parameters. $\hat{J}_{\mathrm{Dy}(1)}$ and $\hat{S}_{\mathrm{Dy}(1)}$ are the spin−orbit and spin-only states for Dy^{3+}, respectively. Fitting of $\chi_M T(T)$ yields $J_{\mathrm{Lines}} = 0.292(1)$ K (0.203(1) cm^{-1}) and 0.226(1) K (0.157(1) cm^{-1}) for **2** and **3a**, respectively (see Figure 4). Fitting the $\chi_M T(T)$ for **1** also reveals an antiferromagnetic interaction ($J_{\mathrm{Lines}} = 2.38(3)$ K (1.65(2) cm^{-1})) operating between the ions.

A direct comparison between J_{ex} and J_{Lines} is not possible; however, the crossings between the antiferromagnetic ground state and the ferromagnetic excited state are reproduced in the Lines model and when considering the low-lying doublets and the interaction obtained directly from the μSQUID analysis (cf. Figures 7 and S18). The J_{Lines} can also be scaled to an $m_J = 15/2$ state, leading to values in excellent agreement with that obtained directly from the μSQUID data $J_{\mathrm{Lines}}(m_J = 15/2) = 32$ mK (0.022 cm^{-1}) for **2** and $J_{\mathrm{Lines}}(m_J = 15/2) = 25$ mK (0.017 cm^{-1}) for **3a** [cf. $J_{ex} = 36$ mK (0.025 cm^{-1}) and $J_{ex} = 26$ mK (0.018 cm^{-1}) for **2** and for **3a**, respectively]. Considering the intramolecular Dy···Dy contact for both complexes (3.782(1) Å for **2** and 3.7255(9) Å for **3a**), the dipolar interaction is found to be $D^{\mathrm{dip}}_{zz} = 20$ mK (0.014 cm^{-1}) for **2** and 21 mK (0.015 cm^{-1}) for **3a**; hence, the interaction operating within the complex might be solely dipolar. Note that a broad

transition centered at +0.38 T is observed for **3a**, which can be ascribed to relaxation via the direct process.

Now, armed with an understanding of the electronic properties of the complexes, it is possible to rationalize the static and dynamic behavior. The single ion character of Dy^{3+} is responsible for the SMM characteristics in all complexes. However, at the single-ion level, the magnetic characteristics of these systems would be dominated by QTM, as is often observed in μSQUID studies. In contrast for **2** and **3a**, the interaction between the Dy^{3+} pairs causes the zero-field QTM process to shift away from zero fields to higher fields, as evidenced by the S-shaped μSQUID loops. Note that the ground-coupled state is not magnetic due to the antiferromagnetic interaction; hence, no SMM properties would be expected in this situation. However, the separation between the ground doublet in both systems is ca. 2 cm^{-1}; thus, the first excited of the coupled system is considerably populated even at 2 K (~24%), causing the response observed in the AC data. Moreover, AC data analysis shows that the barrier for **2** is 107(4) K (74(3) cm^{-1}), which is smaller than the separation of the first excited coupled state and the second excited coupled state lying at ~218 cm^{-1} above it. The lower U_{eff} along with the $\tau(T)$ analysis demonstrate that under-barrier processes play a major role in the relaxation characteristics of **2**.[41] In the case of **3a**, a U_{eff} = 283(43) K (197(30) cm^{-1}) value was obtained. This indicates that relaxation in this coupled system occurs between the first and second excited states of the antiferromagnetically coupled system lying at ~325 cm^{-1}. Furthermore, likewise, **2**, in **3a**, other relaxation pathways are also operative, however, less prominently, as evidenced by their contribution to the $\tau(T)$. The difference in the relaxation characteristics for **2** and **3a** can be a consequence of the ligand fields in which the systems are embedded.

Based on the single-ion CASSCF calculations, it is possible to observe that a higher purity of the ground state wave function and the largest ground to first excited-state separation is achieved for **2** compared to **3a** (see Tables S6–S8). This suggests better performance for **2** than **3a**, which contrasts with our experimental observations. A better insight into the relaxation characteristic of the system can be gained by delving into the transition matrix elements, acting as a proxy for the relaxation. As can be observed in Tables S12–S14, although **2** shows a larger purity of the wave function and larger ground to first excited-state separation, the transition matrix elements are larger for this compound than those found for **3a**, clearly highlighting a slower relaxation mechanism for **3a**. These results are in line with the observed AC data for **3a**, which spans from 2 to 24 K (cf. **2** spanning from 2 to 13 K). In the dimer, the fast active relaxation mechanisms would prompt **2** to relax through the second excited state of the coupled system. Experimentally, a barrier of 107 K was obtained for **2**, which is much lower than the separation between the first excited state and the second excited state, indicating that under-barrier processes are operative.[41] Conversely, the smaller transition matrix elements in **3a** showcase slower relaxation characteristics than those in **2**. A comparison of the experimental barrier for **3a** and the separation between the first excited state of the antiferromagnetically coupled system and the second excited state shows that in this system, relaxation occurs through the second excited state. Based on these findings, we can ascribe the relaxation characteristics to a more axial ligand field in **3a** compared to that in **2**. Note that although Dy^{3+} in **2** has a lower coordination number than in **3a**, Dy^{3+} in **2** is highly irregular (see Figure 3 and the SHAPE factor in the Supporting Information), while Dy^{3+} in **3a** is closer to a D_{3h} geometry. This, along with the ligand field in which Dy^{3+} is embedded, yields a better performance for **3a**.

Similarly, the relaxation behavior of **1** arises from the anisotropic character of the Dy^{3+} ions. Fitting the magnetic data for this system also reveals an antiferromagnetic interaction, while sub-Kelvin μSQUID studies reveal open hysteresis loops. In general, the relaxation dynamics are faster for this system (compared to **2** and **3a**), as evidenced by the $\tau(T)$ and $\chi''(\nu;T)$ characteristics. In contrast, the open loops observed in the μSQUID investigations are a direct consequence of the noncollinear arrangement of the spins of the ground-state properties, which can lead to an overall ferromagnetic ground state.[37] Overall, complex **1** exhibits less prominent SMM behavior than binuclear dysprosium complexes with similar multiple chloride-bridging bonds.[42] Unfortunately, the complex nature of the system [two distinctly oriented molecules residing in the unit cell] prevents us from performing a quantitative analysis since the precise direction of the applied magnetic field is unknown.

CONCLUSIONS

Dimeric mixed-ligand complexes of rare-earth elements ligated by β-diketiminato and catecholate ligands were prepared by salt metathesis in a two-step procedure. In each case, catecholates act as bridging ligands. In dependence on the steric demand of the β-diketiminato ligands, either nonsolvated $[L^1Dy(\mu\text{-}3,5\text{-}Cat)]_2$ (**2**) or THF-coordinated complexes $[L_2Ln(\mu\text{-}3,5\text{-}Cat)(THF)]_2$ (Ln = Dy (**3a**), Y (**3b**)) are formed. The solid-state structures of all substances were determined by single-crystal X-ray diffraction. Magnetic studies reveal anisotropic SMM characteristics for the Dy^{3+} systems. Sub-Kelvin μSQUID loops confirm the SMM behavior of the system. While for **2** and **3a**, the zero-field QTM process is shifted to larger fields, thanks to the interaction between the Dy^{3+} ions, for chloride-bridged dimer $[L^1ClDy(\mu\text{-}Cl)_3DyL^1(THF)]$ (**1**) open loops were found. The latter can be ascribed to the noncollinear arrangements of the easy axes of the Dy^{3+} ions, which can induce an overall ferromagnetic ground state. Sterically hindered 3,5-di-*tert*-butyl-catecholates were found to be effective bridges to build dinuclear lanthanide SMMs, in which the bridging ligands and terminal β-diketiminates possess a great potential to modulate intramolecular interactions and individual local symmetries to enhance SMM properties.

EXPERIMENTAL SECTION

General Considerations. All manipulations of air-sensitive materials were performed with the rigorous exclusion of oxygen and moisture in flame-dried Schlenk-type glassware either on a dual-manifold Schlenk line, interfaced to a high vacuum (10^{-3} mbar) line, or in an argon-filled MBraun glovebox or Korea Kiyon KK-021AS glovebox. THF was distilled under nitrogen from potassium benzophenone ketyl prior to use. Hydrocarbon solvents (*n*-pentane, *n*-heptane, and toluene) were dried using an MBraun solvent purification system (SPS-800). All solvents for vacuum line manipulations were stored in vacuo over the Na/K alloy in resealable flasks. IR spectra were obtained on a Bruker FTIR Tensor 37 through the attenuated total reflection method (ATR) (for **1** and **3a,b**) and in a KBr pellet by means of a FT-801 Fourier spectrometer (Simex) (for **2**). Elemental analyses (CHN) were carried out with an Elementar Micro Cube (for **1** and **3a,b**) and a Euro EA 3000 analyzer (EuroVector) (for **2**). KH was purchased from Aldrich and used as

received. Anhydrous $LnCl_3$,[43] KL^1,[44] and KL^2[25] as well as $[L^2LnCl_2(THF)_2]$ (Ln = Dy, Y)[25] were prepared according to literature procedures. Magnetic susceptibility data on solid samples were collected by using a Quantum Design MPMS-XL SQUID magnetometer. The data were obtained for microcrystalline samples restrained within a polycarbonate gel capsule and corrected for the underlying diamagnetism.

Synthesis of $[L^1ClDy(\mu\text{-}Cl)_3DyL^1(THF)]$ (1). A mixture of $DyCl_3$ (0.55 g, 2.0 mmol) and KL^1 (0.92 g, 2.0 mmol) in THF (50 mL) was stirred at 65 °C for 48 h. Then, THF was removed in vacuo, and the residue was treated with toluene (40 mL). The resulting yellow-green solution was filtered from KCl. The filtrate was concentrated to 15 mL, and 30 mL of *n*-pentane was carefully layered over the pale-yellow-green solution in toluene. The resulting mixture was allowed to store at room temperature. Within 3 weeks, pale-yellow-green X-ray-suitable crystals of $\mathbf{1}\cdot C_6H_5CH_3$ were formed and collected by filtration (1.07 g, yield 73%). Anal. calcd (%) for $C_{69}H_{98}N_4OCl_4Dy_2$ (1466.34): C 56.52, H 6.74, N 3.82. Found C 56.51, H 7.36, N 3.81. IR (ATR) ν, cm^{-1}: 700(w), 729(w), 756(m), 798(m), 934(w), 1022(m), 1059(w), 1100(w), 1174(m), 1254(m), 1276(m), 1292(m), 1322(m), 1362(m), 1382(m), 1438(m), 1460(m), 1522(s), 1548(s), 1592(w), 1621(m), 2868(m), 2925(m), 2959(s).

Synthesis of $[L^1Dy(\mu\text{-}3,5\text{-}Cat)]_2$ (2). A solution of 3,5-$CatK_2$ in THF (15 mL) (obtained by the exhaustive reduction of 3,5-DTBQ (0.110 g, 0.5 mmol) with an excess of potassium) was added to solutions of $[L^1ClDy(\mu\text{-}Cl)_3LnL^1(THF)]$ (0.343 g; 0.25 mmol) in THF (20 mL) resulting in the nearly colorless solutions and the gradual precipitation of KCl. The mixtures were stirred for 48 h at room temperature, and then KCl was removed by filtration. After evaporation of THF to dryness, the residues were treated with *n*-hexane (10 mL) two times. The following careful extraction with *n*-hexane led to the formation of complex **2** (0.176 g, yield 44%) as pale-yellow-green crystals suitable for X-ray analysis. Anal. calcd (%) for $C_{86}H_{122}N_4O_4Dy_2$ (1600.92): C 64.52, H 7.68, N 3.50. Found: C 63.94, H 7.43, N 3.45. IR ν, cm^{-1}: 551(w), 595(w), 629(w), 666(m), 701(w), 757(m), 788(m), 812(m), 831(m), 849(w), 927(m), 973(s), 1024(m), 1056(w), 1106(m), 1170(s), 1203(w), 1235(m), 1254(s), 1316(s), 1362(s), 1383(s), 1393(s), 1412(s), 1437(s), 1460(s), 1512(s), 1552(s), 1584(w), 1623(s), 1645(m), 2867(s), 3059(w).

Synthesis of $[L^2Ln(\mu\text{-}3,5\text{-}Cat)(THF)]_2$ (Ln = Dy (3a), Y (3b)). A solution of 3,5-$CatNa_2$ in THF (15 mL) (obtained by the exhaustive reduction of 3,5-DTBQ (0.055 g, 0.25 mmol) with an excess of sodium) was added to solutions of $[L^2LnCl_2(THF)_2]$ (Ln = Dy, 0.178 g; Y, 0.159 g; 0.25 mmol) in THF (20 mL) resulting in the nearly colorless solutions and gradual precipitation of NaCl. The mixtures were stirred for 48 h at room temperature, and then NaCl was removed by filtration. The slow evaporation of THF from the filtrate afforded the complexes **3a** (0.067 g, yield 34%) and **3b** (0.055 g, yield 31%), respectively, as nearly colorless crystals suitable for X-ray analysis. These crystals were collected by filtration, carefully washed with THF, and dried in vacuo. Following the procedure described for **2**, further workup of the THF mother liquor gave another crop of the corresponding complexes (nearly 15%), which crystallized in different space groups like polymorph **3a′**.

3a: Anal. calcd (%) for $C_{82}H_{114}N_4O_6Dy_2$ (1576.81): C 62.46, H 7.29, N 3.55. Found: C 62.28, H 7.21, N 3.45. IR (ATR) ν, cm^{-1}: 442(w), 478(w), 505(w), 532(w), 546(w), 568(w), 588(w), 635(w), 650(w), 667(w), 743(w), 768(w), 808(w), 827(w), 853(m), 876(w), 914(w), 964(m), 1024(m), 1072(w), 1112(w), 1144(m), 1172(w), 1194(m), 1231(m), 1252(s), 1308(m), 1381(s), 1414(s), 1437(s), 1476(s), 1524(s), 1550(s), 1624(w), 2858(s), 2918(s), 2945(s).

3b: Anal. calcd (%) for $C_{82}H_{114}N_4O_6Y_2$ (1429.62): C 68.89, H 8.04, N 3.92. Found: C 68.82, H 7.96, N 3.77. IR (ATR) ν, cm^{-1}: 446(w), 482(w), 505(w), 532(w), 546(w), 569(w), 590(w), 635(w), 650(w), 667(w), 743(w), 768(w), 808(w), 827(w), 854(m), 879(w), 914(w), 964(m), 1022(m), 1072(w), 1114(w), 1144(m), 1172(w), 1194(m), 1231(m), 1254(s), 1308(m), 1379(s), 1414(s), 1437(s), 1476(s), 1524(s), 1550(s), 1624(w), 2862(s), 2909(s), 2945(s).

X-ray Crystallographic Studies of 1−3. A suitable crystal was covered with mineral oil (Aldrich) and mounted on a glass fiber. The crystal was transferred directly to a cold stream of a Stoe IPDS 2 or Stoe STADI-VARI diffractometer (**1** and **3a,b**).

All structures were solved by using SHELXS/T.[45] The remaining non-hydrogen atoms were located from difference in Fourier map calculations. The refinements were carried out by using full-matrix least-squares techniques on $|F|^2$, using the program SHELXL-2013.[45] Carbon-bonded hydrogen-atom positions were calculated. The locations of the largest peaks in the final difference Fourier map calculation, as well as the magnitude of the residual electron densities in each case, were of no chemical significance.

The crystal structures of **2** and **3a′** were determined by X-ray analysis in an essentially routine way on an Xcalibur diffractometer (Agilent Technologies), using graphite-monochromated Mo$K\alpha$ (λ = 0.71073 Å) radiation. The reflection intensities were measured by the φ-scanning of narrow (0.5°) frames. Empirical absorption correction was applied with the SCALE3 ABSPACK program.[46] The structure was solved by a direct method and refined with full-matrix least-squares treatment against $|F|^2$ in anisotropic approximation for non-hydrogen atoms using SHELX 2014/7 in the ShelXle user surface.[45,47]

The phase purity of compounds **2** and **3a** is evaluated and confirmed using the powder-XRD technique with a STOE X-ray Powder diffractometer (Cu Kα radiation (λ = 1.54184 Å) at 293 K). The powdered samples were measured in the 0.5 mm thick capillaries.

Accession Codes

Deposition Numbers 1570433, 1570435−1570437, and 1570781 contain the supplementary crystallographic data for this paper. These data can be obtained free of charge via the joint Cambridge Crystallographic Data Centre (CCDC) and Fachinformationszentrum Karlsruhe Access Structures service.

AUTHOR INFORMATION

Corresp onding Authors

Svetlana V. Klementyeva − *Institute of Nanotechnology, Karlsruhe Institute of Technology (KIT) Campus North, Karlsruhe 76021, Germany;* orcid.org/0000-0002-0902-3773; Email: svetlana.klementyeva@kit.edu

Mario Ruben − *Institute of Nanotechnology, Karlsruhe Institute of Technology (KIT) Campus North, Karlsruhe 76021, Germany*; Email: mario.ruben@kit.edu

Wolfgang Wernsdorfer − *Physical Institute, Karlsruhe Institut of Technology (KIT) Campus South, Karlsruhe 76131, Germany;* orcid.org/0000-0003-4602-5257; Email: wolfgang.wernsdorfer@kit.edu

Eufemio Moreno-Pineda − *Physical Institute, Karlsruhe Institut of Technology (KIT) Campus South, Karlsruhe 76131, Germany; Departamento de Química-Física, Escuela de Química, Facultad de Ciencias Naturales, Exactas y Tecnología and Facultad de Ciencias Naturales, Exactas y Tecnología, Grupo de Investigación de Materiales, Universidad de Panamá, Panama 0824, Panama;* orcid.org/0000-0002-9643-0341; Email: eufemio.pineda@kit.edu

Authors

Michael T. Gamer – *Institute of Inorganic Chemistry, Karlsruhe Institute of Technology (KIT) Campus South, Karlsruhe 76131, Germany*

Michael Schulze – *Physical Institute, Karlsruhe Institut of Technology (KIT) Campus South, Karlsruhe 76131, Germany*

Nithin Suryadevara – *Institute of Nanotechnology, Karlsruhe Institute of Technology (KIT) Campus North, Karlsruhe 76021, Germany;* orcid.org/0000-0002-8193-3878

Artem S. Bogomyakov – *International Tomography Center SB RAS, Novosibirsk 630090, Russia;* orcid.org/0000-0002-6918-5459

Pavel A. Abramov – *Nikolaev Institute of Inorganic Chemistry SB RAS, Novosibirsk 630090, Russia;* orcid.org/0000-0003-4479-5100

Sergey N. Konchenko – *Institute of Inorganic Chemistry, Karlsruhe Institute of Technology (KIT) Campus South, Karlsruhe 76131, Germany; Nikolaev Institute of Inorganic Chemistry SB RAS, Novosibirsk 630090, Russia; Novosibirsk State University, Novosibirsk 630090, Russia;* orcid.org/0000-0001-8206-2835

Author Contributions

S.V.K.—synthesis of compounds **2** and **3a,b**, writing of original draft, and supervision of the project; S.N.K.—synthesis of compound **1**; M.S., N.S., A.S.B., M.R., and W.W.—measurement and interpretation of magnetic data; M.T.G. and P.A.A.—single-crystal X-ray diffraction analysis; E.M.-P.—theoretical calculations and interpretation of magnetic data and writing of the original draft. The manuscript was written through the contributions of all authors. All authors have given approval to the final version of the manuscript.

Notes

The authors declare no competing financial interest.

ACKNOWLEDGMENTS

We acknowledge the DFG-CCR 1573 "4f for future" (project B3) and the Karlsruhe Nano Micro Facility (KNMF, www.kit.edu/knmf) for the provision of access to instruments at their laboratories. W.W. thanks the German Research Foundation (DFG) for the Gottfried Wilhelm Leibniz-Award, ZVN-2020_WE 4458-5. E.M.-P. thanks the Alexander von Humboldt fellowship for experienced researchers for support. S.V.K. thanks DFG (KL 3519/2-1) for financial support. Authors thank Prof. Dr. Peter Roesky for the provided experimental facilities and Sibylle Schneider for single-crystal X-ray diffraction measurements for compounds **3a,b**.

REFERENCES

(1) (a) Bourget-Merle, L.; Lappert, M. F.; Severn, J. R. The Chemistry of β-Diketiminatometal Complexes. *Chem. Rev.* **2002**, *102*, 3031−3066. (b) Mao, W.; Xiang, L.; Chen, Y. Rare earth metal complexes of β-diketiminato ligands bearing pendant nitrogen or oxygen donors. *Coord. Chem. Rev.* **2017**, *346*, 77−90.

(2) (a) Liddle, S. T.; Arnold, P. L. Synthesis and characterization of yttrium complexes supported by the β-diketiminate ligand {ArNC(CH$_3$)CHC(CH$_3$)NAr}$^-$ (Ar = 2,6-Pr$^i_2$C$_6$H$_3$). *Dalton Trans.* **2007**, 3305−3313. (b) Avent, A. G.; Hitchcock, P. B.; Khvostov, A. V.; Lappert, M. F.; Protchenko, A. V. Synthesis and structures of the ytterbium(II) β-diketiminates [Yb{N(SiMe$_3$)C(R^2)C(H)C(R^4)N(SiMe$_3$)}$_2$] (R^2 = R^4 = Ph, C$_6$H$_4$Me-4, or C$_6$H$_4$Ph-4; or R^2 = C$_6$H$_4$Me-4, R^4 = 1-adamantyl). *Dalton Trans.* **2003**, 1070−1075.

(3) (a) Shen, X.; Zhang, Y.; Xue, M.; Shen, Q. Reduction of sterically hindered β-diketiminato europium(III) complexes by the β-diketiminato anion: a convenient route for the synthesis of β-diketiminato europium(II) complexes. *Dalton Trans.* **2012**, *41*, 3668−3674. (b) Jiao, R.; Shen, X.; Xue, M.; Zhang, Y.; Yao, Y.; Shen, Q. New reaction of β-diketiminatoeuropium complex: sterically induced oxidation−coupling of β-diketiminato ligands. *Chem. Commun.* **2010**, *46*, 4118−4120. (c) Jiao, R.; Xue, M. Q.; Shen, X. D.; Zhang, Y.; Yao, Y. M.; Shen, Q. A. comparative study on the reactivity of tris-β-diketiminate ytterbium complexes: steric effect of β-diketiminato ligands. *Eur. J. Inorg. Chem.* **2010**, *2010*, 2523−2529. (e) Mironova, O. A.; Sukhikh, T. S.; Konchenko, S. N.; Pushkarevsky, N. A. Structural Diversity and Multielectron Reduction Reactivity of Samarium(II) Iodido-β-diketiminate Complexes Dependent on Tetrahydrofuran Content. *Inorg. Chem.* **2022**, *61*, 15484−15498. (f) Mironova, O. A.; Sukhikh, T. S.; Konchenko, S. N.; Pushkarevsky, N. A. Study of the Possibility of Using Salt Metathesis Reactions for the Synthesis of the Neodymium and Samarium β-Diketiminate Chalcogenide Complexes. Unexpected Reduction of Sm(III) to Sm(II). *Russ. J. Coord. Chem.* **2020**, *46*, 241−250.

(4) (a) Thakur, S. K.; Roig, N.; Monreal-Corona, R.; Langer, J.; Alonso, M.; Harder, S. Similarities and Differences in Benzene Reduction with Ca, Sr, Yb and Sm: Strong Evidence for Tetra-Anionic Benzene. *Angew. Chem., Int. Ed.* **2024**, *63* (25), No. e202405229. (b) Wang, Y.; Zhang, Y.; Liang, J.; Tan, B.; Deng, C.; Huang, W. Neutral inverse-sandwich rare-earth metal complexes of the benzene tetraanion. *Chem. Sci.* **2024**, *15*, 8740−8749. (c) Schmid, M.; Guillaume, S. M.; Roesky, P. W. β-Diketiminate rare earth borohydride complexes: synthesis, structure, and catalytic activity in the ring-opening polymerization of ε-caprolactone and trimethylene carbonate. *Organometallics* **2014**, *33*, 5392−5401. (d) Li, D.; Li, S.; Cui, D.; Zhang, X. β-Diketiminato Rare earth Metal Complexes. Structures, Catalysis, and Active Species for Highly cis-1,4-Selective Polymerization of Isoprene. *Organometallics* **2010**, *29* (9), 2186−2193.

(5) (a) Mironova, O. A.; Ryadun, A. A.; Sukhikh, T. S.; Konchenko, S. N.; Pushkarevsky, N. A. Synthesis and luminescence studies of lanthanide complexes (Gd, Tb, Dy) with phenyl- and 2-pyridylthiolates supported by a bulky β-diketiminate ligand. Impact of the ligand environment on terbium(iii) emission. *New J. Chem.* **2020**, *44*, 19769−19779. (b) Mironova, O. A.; Sukhikh, T. S.; Konchenko, S. N.; Pushkarevsky, N. A. Synthesis, structural and IR spectral studies of lanthanide (Nd, Sm) phenyl- and 2-pyridylthiolates supported by bulky 2,6-diisopropylphenyl substituted β-diketiminate ligand. *Polyhedron* **2019**, *159*, 337−344. (c) Kenward, A. L.; Piers, W. E.; Parvez, M. Low-coordinate organoyttrium complexes supported by β-diketiminato ligands. *Organometallics* **2009**, *28*, 3012−3020. (d) Wei, X.; Cheng, Y.; Hitchcock, P. B.; Lappert, M. F. Syntheses, structures and reactions of a series of β-diketiminatoyttrium compounds. *Dalton Trans.* **2008**, 5235−5246. (e) Yao, Y.; Zhang, Z.; Peng, H.; Zhang, Y.; Shen, Q.; Lin, J. Synthesis and Structural Characterization of β-Diketiminate−Lanthanide Amides and Their Catalytic Activity for the Polymerization of Methyl Methacrylate and ε-Caprolactone. *Inorg. Chem.* **2006**, *45* (5), 2175−2183. (f) Luo, Y.-J.; Yao, Y.-M.; Zhang, Y.; Shen, Q.; Yu, K.-B. Synthesis, reactivity and crystal structure of β-diketiminate ytterbium chlorides. *Chin. J. Chem.* **2004**, *22*, 187−190. (g) Neculai, D.; Roesky, H. W.; Neculai, A. M.; Magull, J.; Herbst-Irmer, R.; Walfort, B.; Stalke, D. The first β-diketiminato complex of terbium containing two alkyl groups: a model compound for LLnR$_2$ (Ln = lanthanide, R = alkyl) systems. *Organometallics* **2003**, *22*, 2279−2283. (h) Yao, Y.; Xue, M.; Luo, Y.; Zhang, Z.; Jiao, R.; Zhang, Y.; Shen, Q.; Wong, W.; Yu, K.; Sun, J. Synthesis and characterization of β-diketiminate lanthanide complexes: the effect of the bulkiness of ancillary ligand on the reaction. *J. Organomet. Chem.* **2003**, *678*, 108−116. (i) Zhang, Y.; Yao, Y. M.; Luo, Y. J.; Shen, Q.; Cui, Y.; Yu, K. B. Ytterbium complexes supported

by β-diketiminate ligands: cyclopentadienyl, indenyl, and aryloxide derivatives. *Polyhedron* **2003**, *22*, 1241−1247.
(6) Camp, C.; Arnold, J. On the non-innocence of "Nacnacs": ligand-based reactivity in β-diketiminate supported coordination compounds. *Dalton Trans.* **2016**, *45*, 14462−14498.
(7) (a) Pushkarevsky, N. A.; Ogienko, M. A.; Smolentsev, A. I.; Novozhilov, I. N.; Witt, A.; Khusniyarov, M. M.; Cherkasov, V. K.; Konchenko, S. N. Cooperative reduction by Ln^{2+} and Cp^{*-}ions: synthesis and properties of Sm, Eu, and Yb complexes with 3,6-di-tert-butyl-o-Benzoquinone. *Dalton Trans.* **2016**, *45*, 1269−1278. (b) Sinitsa, D. K.; Sukhikh, T. S.; Konchenko, S. N.; Pushkarevsky, N. A. P. Structural Variety, Isomerism, and Interconversions of Polynuclear Samarium Complexes with Reduced 9,10-Phenanthrenequinone Ligand. *Organometallics* **2024**, *43* (2), 94−107.
(8) Petrov, P. A.; Samsonenko, D. G. Yttrium complexes with 3,6-bis(tert-butylcatecholate). *Russ. J. Coord. Chem.* **2017**, *43*, 500−504.
(9) (a) Pointillart, F.; Klementieva, S. V.; Kuropatov, V. A.; Le Gal, Y.; Golhen, S.; Cador, O.; Cherkasov, V. K.; Ouahab, L. A single molecule magnet behavior in a D_{3h} symmetry Dy(III) complex involving a quinone−tetrathiafulvalene−quinone bridge. *Chem. Commun.* **2012**, *48*, 714−716. (b) Pointillart, F.; Kuropatov, V. A.; Mitin, A. S.; Maury, O.; Le Gal, Y.; Golhen, S.; Cador, O.; Cherkasov, V. K.; Ouahab, L. Lanthanide-based dinuclear complexes involving an *o*-quinone−tetrathiafulvalene-*o*-quinone bridging ligand: X-ray structures, magnetic and photophysical properties. *Eur. J. Inorg. Chem.* **2012**, *2012*, 4708−4718.
(10) Kuzyaev, D. M.; Vorozhtsov, D. L.; Druzhkov, N. O.; Lopatin, M. A.; Baranov, E. V.; Cherkasov, A. V.; Fukin, G. K.; Abakumov, G. A.; Bochkarev, M. N. 3,5-Di-tert-butyl-o-benzoquinone complexes of lanthanides. *J. Organomet. Chem.* **2012**, *698*, 35−41.
(11) (a) Caneschi, A.; Dei, A.; Gatteschi, D.; Massa, C. A.; Pardi, L. A.; Poussereau, S.; Sorace, L. Evaluating the magnetic anisotropy in molecular rare earth compounds. Gadolinium derivatives with semiquinone radical and diamagnetic analogues. *Chem. Phys. Lett.* **2003**, *371*, 694−699. (b) Dei, A.; Gatteschi, D.; Pécaut, J.; Poussereau, S.; Sorace, L.; Vostrikova, K. Crystal field and exchange effects in rare earth semiquinone complexes. *Comptes Rendus de l'Acaďemie des Sciences - Series IIC - Chemistry* **2001**, *4*, 135−141. (c) Caneschi, A.; Dei, A.; Gateschi, D.; Sorace, L.; Vostrikova, K. Antiferromagnetic coupling in a gadolinium(III) semiquinonato complex. *Angew. Chem., Int. Ed.* **2000**, *39* (1), 246−248. (d) Dei, A.; Gatteschi, D.; Massa, C. A.; Pardi, L. A.; Poussereau, S.; Sorace, L. Spontaneous symmetry breaking in the formation of a dinuclear gadolinium semiquinonato complex: synthesis, high-field EPR studies, and magnetic properties. *Chem.—Eur. J.* **2000**, *6*, 4580−4586. (e) Caneschi, A.; Dei, A.; Gatteschi, D.; Poussereau, S.; Sorace, L. Antiferromagnetic coupling between rare earth ions and semiquinones in a series of 1 : 1 complexes. *Dalton Trans.* **2004**, 1048−1055. (f) Domingos, A.; Lopes, I.; Waerenborgh, J. C.; Marques, N.; Lin, G. Y.; Zhang, X. W.; Takats, J.; McDonald, R.; Hillier, A. C.; Sella, A.; Elsegood, M. R. G.; Day, V. W. Trapping of anionic organic radicals by $(Tp^{Me2})_2Ln$ (Ln = Sm, Eu). *Inorg. Chem.* **2007**, *46*, 9415−9424.
(12) (a) Bernot, K. Get under the Umbrella: A Comprehensive Gateway for Researchers on Lanthanide-Based Single-Molecule Magnets. *Eur. J. Inorg. Chem.* **2023**, *26*, No. e202300336. (b) Wang, J.; Sun, C.-Y.; Zheng, Q.; Wang, D.-Q.; Chen, Y.-T.; Ju, J.-F.; Sun, T.-M.; Cui, Y.; Ding, Y.; Tang, Y.-F. Lanthanide Single-molecule Magnets: Synthetic Strategy, Structures, Properties and Recent Advances. *Chem.−Asian J.* **2023**, *18*, No. e202201297. (c) Zabala-Lekuona, A.; Seco, J. M.; Colacio, E. Single-Molecule Magnets: From Mn12-ac to dysprosium metallocenes, a travel in time. *Coord. Chem. Rev.* **2021**, *441*, 213984. (d) Shao, D.; Wang, X.-Y. Development of Single-Molecule Magnets. *Chin. J. Chem.* **2020**, *38*, 1005−1018. (e) Zhu, Z.; Guo, M.; Li, X.-L.; Tang, J. Molecular magnetism of lanthanide: Advances and perspectives. *Coord. Chem. Rev.* **2019**, *378*, 350−364. (f) Lu, J.; Guo, M.; Tang, J. Recent Developments in Lanthanide Single-Molecule Magnets. *Chem.—Asian J.* **2017**, *12*, 2772−2779. (g) *Introduction to Molecular Magnetism: From Transition Metals to Lanthanides*; Benelli, C., Gatteschi, D., Eds.; Wiley VCH: Weinheim, 2015; . (h) *Lanthanides and Actinides in Molecular Magnetism*; Layfield, R., Murugesu, M., Eds.; Wiley VCH: Weinheim, 2015; . (i) Dreiser, J. Molecular lanthanide single-ion magnets: from bulk to submonolayers. *J. Phys.: Condens. Matter* **2015**, *27* (1−20), 183203. (j) Layfield, R. A. Organometallic single-molecule magnets. *Organometallics* **2014**, *33*, 1084−1099. (k) Woodruff, D. N.; Winpenny, R. E. P.; Layfield, R. A. Lanthanide single-molecule magnets. *Chem. Rev.* **2013**, *113*, 5110−5148. (l) Rinehart, J. D.; Long, J. R. Exploiting single-ion anisotropy in the design of f-element single-molecule magnets. *Chem. Sci.* **2011**, *2*, 2078−2085. (m) Sorace, L.; Benelli, C.; Gatteschi, D. Lanthanides in molecular magnetism: old tools in a new field. *Chem. Soc. Rev.* **2011**, *40*, 3092−3104.
(13) (a) Vieru, V.; Gómez-Coca, S.; Ruiz, E.; Chibotaru, L. F. Increasing the Magnetic Blocking Temperature of Single-Molecule Magnets. *Angew. Chem., Int. Ed.* **2024**, *63*, No. e202303146. (b) Xu, W.-J.; Luo, Q.-C.; Li, Z.-H.; Zhai, Y.-Q.; Zheng, Y.-Z. Bis-Alkoxide Dysprosium(III) Crown Ether Complexes Exhibit Tunable Air Stability and Record Energy Barrier. *Adv. Sci.* **2024**, *11*, 2308548. (c) Gould, C. A.; McClain, K. R.; Reta, D.; Kragskow, J. G. C.; Marchiori, D. A.; Lachman, E.; Choi, E.-S.; Analytis, J. G.; Britt, R. D.; Chilton, N. F.; Harvey, B. G.; Long, J. R. Ultrahard magnetism from mixed-valence dilanthanide complexes with metal-metal bonding. *Science* **2022**, *375*, 198. (d) Ding, X.-L.; Zhai, Y.-Q.; Han, T.; Chen, W.-P.; Ding, Y.-S.; Zheng, Y.-Z. A Local D4*h* Symmetric Dysprosium-(III) Single-Molecule Magnet with an Energy Barrier Exceeding 2000 K. *Chem.—Eur. J.* **2021**, *27*, 2623−2627. (e) Guo, F.-S.; Day, B. M.; Chen, Y.-C.; Tong, M.-L.; Mansikkamäki, A.; Layfield, R. A. Magnetic hysteresis up to 80 K in a dysprosium metallocene single-molecule magnet. *Science* **2018**, *362*, 1400−1403. (f) Goodwin, C. A. P.; Ortu, F.; Reta, D.; Chilton, N. F.; Mills, D. P. Molecular magnetic hysteresis at 60 K in dysprosocenium. *Nature* **2017**, *548*, 439. (g) Guo, F. S.; Day, B. M.; Chen, Y. C.; Tong, M. L.; Mansikkamäki, A.; Layfield, R. A. A Dysprosium Metallocene Single-Molecule Magnet Functioning at the Axial Limit. *Angew. Chem., Int. Ed.* **2017**, *56*, 11445.
(14) Swain, A.; Sharma, T.; Rajaraman, G. Strategies to quench quantum tunneling of magnetization in lanthanide single molecule magnets. *Chem. Commun.* **2023**, *59*, 3206.
(15) (a) Tian, J.; Du, J.; Li, B.; Zhang, H.; Zhang, Y.; Sun, L.; Ma, P. Recent advances of dinuclear dysprosium-based single-molecule magnets: from mechanisms to application. *J. Mater. Chem. C* **2024**, *12*, 14754−14773. (b) Nguyen, G. T.; Ungur, L. The Role of Radical Bridges in Polynuclear Single-Molecule Magnets. *Chem.—Eur. J.* **2022**, *28*, No. e202200227F. (c) Chen, Y.-C.; Tong, M.-L. Single-molecule magnets beyond a single lanthanide ion: the art of coupling. *Chem. Sci.* **2022**, *13*, 8716. (d) Habib, F.; Murugesu, M. Lessons learned from dinuclear lanthanide nano-magnets. *Chem. Soc. Rev.* **2013**, *42*, 3278−3288.
(16) (a) Li, H.-D.; Wu, S.-G.; Tong, M.-L. Lanthanide−radical single-molecule magnets: current status and future challenges. *Chem. Commun.* **2023**, *59*, 6159. (b) Zhang, P.; Nabi, R.; Staab, J. K.; Chilton, N. F.; Demir, S. Taming Super-Reduced Bi_2^{3-} Radicals with Rare Earth Cations. *J. Am. Chem. Soc.* **2023**, *145* (16), 9152−9163. (c) Mavragani, N.; Kitos, A. A.; Hrubý, J.; Hill, S.; Mansikkamäki, A.; Moilanen, J. O.; Murugesu, M. Strong magnetic exchange coupling in Ln_2 metallocenes attained by the trans-coordination of a tetrazinyl radical ligand. *Inorg. Chem. Front.* **2023**, *10*, 4197. (d) Mavragani, N.; Kitos, A. A.; Mansikkamäki, A.; Murugesu, M. New members of radical bridged Ln_2 metallocene single-molecule magnets based on the unsubstituted 1,2,4,5-tetrazine ligand. *Inorg. Chem. Front.* **2022**, *10*, 259. (e) Benner, F.; La Droitte, L.; Cador, O.; Le Guennic, B.; Demir, S. Magnetic hysteresis and large coercivity in bisbenzimidazole radical-bridged dilanthanide complexes. *Chem. Sci.* **2023**, *14*, 5577. (f) Nguyen, G. T.; Ungur, L. Understanding the magnetization blocking mechanism in N_2^{3-} radical-bridged dilanthanide single-molecule magnets. *Phys. Chem. Chem. Phys.* **2021**, *23*, 10303. (g) Gould, C. A.; Mu, E.; Vieru, V.; Darago, L. E.; Chakarawet, K.; Gonzalez, M. I.; Demir, S.; Long, J. R. Substituent Effects on Exchange Coupling and Magnetic Relaxation in 2,2′-Bipyrimidine Radical-Bridged Dilanthanide Complexes. *J. Am. Chem. Soc.* **2020**,

142, 21197−21209. (h) Demir, S.; Gonzalez, M. I.; Darago, L. E.; Evans, W. J.; Long, J. R. Giant coercivity and high magnetic blocking temperatures for N_2^{3-} radical-bridged dilanthanide complexes upon ligand dissociation. *Nat. Commun.* **2017**, *8*, 2144.

(17) (a) Zhang, P.; Benner, F.; Chilton, N. F.; Demir, S. Organometallic lanthanide bismuth cluster single-molecule magnets. *Chem.* **2022**, *8*, 717−730. (b) Tuna, F.; Smith, C. A.; Bodensteiner, M.; Ungur, L.; Chibotaru, L. F.; McInnes, E. J. L.; Winpenny, R. E. P.; Collison, D.; Layfield, R. A. A High Anisotropy Barrier in a Sulfur-Bridged Organodysprosium Single-Molecule Magnet. *Angew. Chem.* **2012**, *124*, 7082−7086.

(18) (a) Zhang, L.; Ma, H.; Wang, Z.-Q.; Tian, Y.-M.; Zhang, Y.-Q.; Sun, W.-B. Double and triple pyridine-N-oxide bridged dinuclear Dysprosium(III) dimers and single-molecule magnetic properties. *J. Mol. Struct.* **2019**, *1175*, 686−697. (b) Zhang, L.; Chen, P.; Li, H.-F.; Tian, Y.-M.; Yan, P.-F.; Sun, W.-B. Structure and Single-Molecule Magnetic Property of a Dinuclear Dy2 Complex Bridged by the 4-Methylpyridine N-Oxide Ligand. *Eur. J. Inorg. Chem.* **2018**, *2018* (32), 3668−3674. (c) Yi, X.; Bernot, K.; Pointillart, F.; Poneti, G.; Calvez, G.; Daiguebonne, C.; Guillou, O.; Sessoli, R. A Luminescent and Sublimable DyIII-Based Single-Molecule Magnet. *Chem.—Eur. J.* **2012**, *18*, 11379−11387. (d) Pointillart, F.; Le Gal, Y.; Golhen, S.; Cador, O.; Ouahab, L. Single-Molecule Magnet Behaviour in a Tetrathiafulvalene-Based Electroactive Antiferromagnetically Coupled Dinuclear Dysprosium(III) Complex. *Chem.—Eur. J.* **2011**, *17*, 10397−10404.

(19) (a) Yu, S.; Hu, H.; Liu, D.; Liang, Y.; Liang, F.; Yin, B.; Chen, Z. Structural and magnetic studies of six-coordinated Schiff base Dy(III) complexes. *Inorg. Chem. Front.* **2022**, *9*, 3059−3070. (b) Yu, S.; Hu, Z.; Chen, Z.; Li, B.; Zhang, Y.-Q.; Liang, Y.; Liu, D.; Yao, D.; Liang, F. Two Dy(III) Single-Molecule Magnets with Their Performance Tuned by Schiff Base Ligands. *Inorg. Chem.* **2019**, *58* (2), 1191−1200. (c) Ge, Y.; Li, D.; Wang, G.; Cui, Y.; Najib, M. S.; Li, Y.; Wang, B.-L. Single-Molecule Magnetism in Three Dy2 Complexes from the Use of a Pentadentate Schiff Base Ligand and Different Benzoates. *Chem.—Asian J.* **2019**, *14*, 2846−2852. (d) Gao, F.; Zhang, Y.-Q.; Sun, W.; Liu, H.; Chen, X. Syntheses, structures and magnetic properties of macrocyclic Schiff base-supported homodinuclear lanthanide complexes. *Dalton Trans.* **2018**, *47*, 11696−11704. (e) Ge, Y.; Qin, Y.; Cui, Y.; Pan, Y.; Huang, Y.; Li, Y.; Liu, W.; Zhang, Y.-Q. Dinuclear Lanthanide Complexes Based on a Schiff-base Ligand: Free Lattice Solvent Inducing the Single Molecule Magnet Behavior of Dy2 Compound. *Chem.—Asian J.* **2018**, *13*, 3753−3761.

(20) (a) Ma, X.-F.; Huang, X.-D.; Zheng, L.-M. Tuning the Single-Molecule Magnet and Photoluminescence Properties of Binuclear Dysprosium Complexes by Light Published as part of a Crystal Growth and Design virtual special issue on Molecular Magnets and Switchable Magnetic Materials. *Cryst. Growth Des.* **2023**, *23*, 1095−1103. (b) Roy, S.; Shukla, P.; Ahmed, N.; Du, M.-H.; Tarannum, I.; Kong, X.-J.; Gupta, T.; Singh, S. K.; Das, S. Interplay between anisotropy and magnetic exchange to modulate the magnetic relaxation behaviours of phenoxo bridged Dy2 dimers with axial β-diketonate co-ligands. *Dalton Trans.* **2022**, *51*, 18187−18202. (c) Kong, M.; Feng, X.; Wang, J.; Zhang, Y.-Q.; Song, Y. Tuning magnetic anisotropy via terminal ligands along the Dy···Dy orientation in novel centrosymmetric [Dy2] single molecule magnets. *Dalton Trans.* **2021**, *50*, 568−577. (d) Bera, S. P.; Mondal, A.; Konar, S. Investigation of the role of terminal ligands in magnetic relaxation in a series of dinuclear dysprosium complexes. *Inorg. Chem. Front.* **2020**, *7*, 3352−3363. (e) Zhang, W.; Xu, S.-M.; Zhu, Z.-X.; Ru, J.; Zhang, Y.-Q.; Yao, M.-X. Strong intramolecular DyIII − DyIII magnetic couplings up to 15.00 cm^{-1} in phenoxyl-bridged dinuclear 4f complexes. *New J. Chem.* **2020**, *44*, 2083−2090.

(21) Xiong, J.; Ding, H.-Y.; Meng, Y.-S.; Gao, C.; Zhang, X.-J.; Meng, Z.-S.; Zhang, Y.-Q.; Shi, W.; Wang, B.-W.; Gao, S. Hydroxide-bridged five-coordinate DyIII single-molecule magnet exhibiting the record thermal relaxation barrier of magnetization among lanthanide-only dimmers. *Chem. Sci.* **2017**, *8*, 1288−1294.

(22) Harriman, K. L. M.; Murugesu, M. An Organolanthanide Building Block Approach to Single-Molecule Magnets. *Acc. Chem. Res.* **2016**, *49*, 1158−1167.

(23) Hay, M. A.; Boskovic, C. Lanthanoid Complexes as Molecular Materials: The Redox Approach. *Chem.—Eur. J.* **2021**, *27*, 3608−3637.

(24) (a) Zhang, P.; Perfetti, M.; Kern, M.; Hallmen, P. P.; Ungur, L.; Lenz, S.; Ringenberg, M. R.; Frey, W.; Stoll, H.; Rauhut, G.; van Slageren, J. Exchange coupling and single molecule magnetism in redox-active tetraoxolene-bridged dilanthanide complexes. *Chem. Sci.* **2018**, *9*, 1221. (b) Moilanen, J. O.; Mansikkamäki, A.; Lahtinen, M.; Guo, F.-S.; Kalenius, E.; Layfield, R. A.; Chibotaru, L. F. Thermal expansion and magnetic properties of benzoquinone-bridged dinuclear rare-earth complexes. *Dalton Trans.* **2017**, *46*, 13582.

(25) Klementyeva, S. V.; Afonin, M. Yu.; Bogomyakov, A. S.; Gamer, M. T.; Roesky, P. W.; Konchenko, S. N. Mono- and dinuclear rare-earth chlorides ligated by a mesityl-substituted β-diketiminate. *Eur. J. Inorg. Chem.* **2016**, *2016*, 3666−3672.

(26) (a) Klementyeva, S. V.; Sukhikh, T. S.; Abramov, P. A.; Poddel'sky, A. I. Low-Coordinate Mixed Ligand NacNac Complexes of Rare Earth Metals. *Molecules* **2023**, *28*, 1994. (b) Klementyeva, S. V.; Petrov, P. A.; Starikova, A. A.; Konchenko, S. N. Erbium Mixed-Ligand β-Diketiminato-Diamido Complex: Unusual Structure of Diamide Ligand. *ChemistrySelect* **2018**, *3*, 1262−1267. (c) Klementyeva, S. V.; Smolentsev, A. I.; Abramov, P. A.; Konchenko, S. N. Yttrium 3,5-di-tert-butyl-catecholates supported by 2,6-diisopropylphenyl substituted β-diketiminate. *Inorg. Chem. Commun.* **2017**, *86*, 154−158.

(27) (a) Johnson, K. R. D.; Côté, A. P.; Hayes, P. G. Four-coordinate erbium organometallic and coordination complexes: synthesis and structure. *J. Organomet. Chem.* **2010**, *695*, 2747−2755. (b) Cui, C.; Shafir, A.; Schmidt, J. A. R.; Oliver, A. G.; Arnold, J. Synthesis and characterization of mono β-diketiminatosamarium amides and hydrocarbyls. *Dalton Trans.* **2005**, 1387−1393. (c) Yao, Y.; Zhang, Y.; Shen, Q.; Yu, K. Synthesis, reactivity, and structure of mixed-ligand ytterbium complexes supported by β-diketiminate. *Organometallics* **2002**, *21*, 819−824. (d) Sánchez-Barba, L. F.; Hughes, D. L.; Humphrey, S. M.; Bochmann, M. Ligand Transfer Reactions of Mixed-Metal Lanthanide/Magnesium Allyl Complexes with β-Diketimines: Synthesis, Structures, and Ring-Opening Polymerization Catalysis. *Organometallics* **2006**, *25* (4), 1012−1020. (e) Sun, X.; Xie, Z.; Li, S.; Cao, H.; Fan, Y.; Li, P.; Zou, L. Mono-β-diketiminate supported cerium(III) complex: Synthesis, characterization and reactivity. *Polyhedron* **2024**, *249*, 116773−116780. (f) Zhang, Z.-Q.; Yao, Y.-M.; Zhang, Y.; Shen, Q.; Wong, W.-T. Synthesis, characterization and structural diversity of lanthanide chlorides supported by the β-diketiminate ligand $[\{(2,6\text{-}Me_2C_6H_3)\text{-}NC(Me)\}_2CH]^-$. *Inorg. Chim. Acta* **2004**, *357*, 3173−3180.

(28) (a) Zanello, P.; Corsini, M. Homoleptic mononuclear transition metal complexes of 1,2-dioxolenes: Updating their electrochemical-to-structural (X-ray) properties. *Coord. Chem. Rev.* **2006**, *250* (15−16), 2000−2022. (b) Scherer, T. M.; Hartenbach, I.; Lissner, F.; Schwederski, B.; Hübner, R.; Fiedler, J.; Záliš, S.; Sarkar, B.; Kaim, W. Analysis of Multiple Redox Sites in Complexes $[M(C_5Me_5)(Q)\text{-}(NO)]_n$, M = Ru or Os, Q = o-Quinones. *Z. Anorg. Allg. Chem.* **2021**, *647* (8), 867−875. (c) Astaf'eva, T. V.; Rumyantcev, R. V.; Arsenyev, M. V.; Zherebtsov, M. A.; Fukin, G. K.; Cherkasov, V. K.; Poddel'sky, A. I. 1D Coordination polymers based on triphenylantimony(V) 3-formyl-substituted catecholates. *J. Organomet. Chem.* **2022**, *958*, 122190. (d) Poddel'sky, A. I.; Astaf'eva, T. V.; Smolyaninov, I. V.; Arsenyev, M. V.; Fukin, G. K.; Berberova, N. T.; Cherkasov, V. K.; Abakumov, G. A. Triphenylantimony(V) 6-alkoxymethyl-3,5-di-tert-butylcatecholates. Structure and redox-properties. *J. Organomet. Chem.* **2018**, *873*, 57−65. (e) Brown, S. N. Metrical Oxidation States of 2-Amidophenoxide and Catecholate Ligands: Structural Signatures of Metal−Ligand π Bonding in Potentially Noninnocent Ligands. *Inorg. Chem.* **2012**, *51* (3), 1251−1260.

(29) (a) Beattie, R. J.; Sutton, A. D.; Scott, B. L.; Clark, D. L.; Kiplinger, J. L.; Gordon, J. C. Lutetium functionalities supported by a sterically encumbered β-diketiminate ligand. *J. Organomet. Chem.*

2018, *857*, 187−190. (b) Neculai, A. M.; Neculai, D.; Roesky, H. W.; Magull, J. Synthesis and structure of $LLnBr_2$ (L = $Et_2NCH_2CH_2NC(Me)CHC(Me)NCH_2CH_2NEt_2$; Ln = Y, Sm, and Yb). *Polyhedron* **2004**, *23*, 183−187. (c) Nikiforov, G. B.; Roesky, H. W.; Labahn, T.; Vidovic, D.; Neculai, D. Synthesis and structure of the first holmium and erbium diiodide complexes of composition $LLnI_2$ (Ln = Ho, Er). *Eur. J. Inorg. Chem.* **2003**, *2003*, 433−436. (d) Neculai, A. M.; Neculai, D.; Nikiforov, G.; Roesky, H. W.; Magull, J.; Schlicker, C.; Herbst-Irmer, R.; Noltemeyer, M. Partially fluorinated rare earth metal complexes. *Eur. J. Inorg. Chem.* **2003**, *2003*, 3120−3126. (e) Yao, Y. M.; Luo, Y. J.; Jiao, R.; Shen, Q.; Yu, K. B.; Weng, L. H. Synthesis of lanthanide chlorides supported by β-diketiminate ligands and molecular structures of $L^1SmCl_2(THF)_2$ and $L^2SmCl_2(THF)_2$ [L^1 = PhNC(Me)CHC(Me)NPh; L^2 = *p*-ClPhNC(Me)CHC(Me)-NPh(2,6-Pr^i_2)]. *Polyhedron* **2003**, *22*, 441−446. (f) Neculai, D.; Roesky, H. B.; Neculai, A. M.; Magull, J.; Schmidt, H.-G.; Noltemeyer, M. Synthesis and structure of monomeric and solvent-free $LPrX_2$ compounds supported by a new β-diketiminato ligand [L = $Et_2NCH_2CH_2NC(Me)CHC(Me)NCH_2CH_2NEt_2$, X = Cl, Br, BH_4]. *J. Organomet. Chem.* **2002**, *643*, 47−52. (g) Drees, D.; Magull, J. Neue Komplexe der Lanthanoiden mit zweizähnigen Liganden. Die Strukturen von $[(C_{17}H_{17}N_2)GdBr_2(thf)_2]$ und $[(C_{17}H_{17}N_2)_3Ln]$ (L = Sm, Gd). *Z. Anorg. Allg. Chem.* **1994**, *620*, 814−818.

(30) (a) Pinsky, M.; Avnir, D. Continuous Symmetry Measures. 5. The Classical Polyhedra. *Inorg. Chem.* **1998**, *37*, 5575−5582. (b) Casanova, D.; Cirera, J.; Llunell, M.; Alemany, P.; Avnir, D.; Alvarez, S. Minimal Distortion Pathways in Polyhedral Rearrangements. J. *Am. Chem. Soc.* **2004**, *126*, 1755−1763.

(31) (a) Moreno-Pineda, E.; Godfrin, C.; Balestro, F.; Wernsdorfer, W.; Ruben, M. Molecular spin qudits for quantum algorithms. *Chem. Soc. Rev.* **2018**, *47*, 501−513. (b) Moreno-Pineda, E.; Wernsdorfer, W. Measuring molecular magnets for quantum technologies. *Nat. Rev. Phys.* **2021**, *3*, 645−659. (c) Atzori, M.; Sessoli, R. The Second Quantum Revolution: Role and Challenges of Molecular Chemistry. *J. Am. Chem. Soc.* **2019**, *141*, 11339−11352. (d) Coronado, E. Molecular magnetism: from chemical design to spin control in molecules, materials and devices. *Nat. Rev. Mater.* **2020**, *5*, 87−104.

(32) (a) Münzfeld, L.; Dahlen, M.; Hauser, A.; Mahieu, N.; Kuppusamy, S. K.; Moutet, J.; Tricoire, M.; Köppe, R.; La Droitte, L.; Cador, O.; Le Guennic, B.; Nocton, G.; Moreno-Pineda, E.; Ruben, M.; Roesky, P. W. Molecular Lanthanide Switches for Magnetism and Photoluminescence. *Angew. Chem., Int. Ed.* **2023**, *62*, No. e202218107. (b) Goodwin, C. A. P.; Reta, D.; Ortu, F.; Chilton, N. F.; Mills, D. P. Synthesis and Electronic Structures of Heavy Lanthanide Metallocenium Cations. *J. Am. Chem. Soc.* **2017**, *139*, 18714−18724.

(33) (a) Garlatti, E.; Albino, A.; Chicco, S.; Nguyen, V. H. A.; Santanni, F.; Paolasini, L.; Mazzoli, C.; Caciuffo, R.; Totti, F.; Santini, P.; Sessoli, R.; Lunghi, A.; Carretta, S. The critical role of ultra-low-energy vibrations in the relaxation dynamics of molecular qubits. *Nat. Commun.* **2023**, *14*, 1653. (b) Briganti, M.; Santanni, F.; Tesi, L.; Totti, F.; Sessoli, R.; Lunghi, A. A Complete Ab Initio View of Orbach and Raman Spin−Lattice Relaxation in a Dysprosium Coordination Compound. *J. Am. Chem. Soc.* **2021**, *143* (34), 13633−13645.

(34) (a) Santana, F. S.; Perfetti, M.; Briganti, M.; Sacco, F.; Poneti, G.; Ravera, E.; Soares, J. F.; Sessoli, R. A dysprosium single molecule magnet outperforming current pseudocontact shift agents. *Chem. Sci.* **2022**, *13*, 5860−5871. (b) Wang, J.; Zakrzewski, J. J.; Zychowicz, M.; Xin, Y.; Tokoro, H.; Chorazy, S.; Ohkoshi, S. Desolvation-Induced Highly Symmetrical Terbium(III) Single-Molecule Magnet Exhibiting Luminescent Self-Monitoring of Temperature. *Angew. Chem., Int. Ed.* **2023**, *62* (35), No. e202306372. (c) Uhlmann, C.; Münzfeld, L.; Hauser, A.; Ruan, T.-T.; Kumar Kuppusamy, S.; Jin, C.; Ruben, M.; Fink, K.; Moreno-Pineda, E.; Roesky, P. W. Unique Double and Triple Decker Arrangements of Rare-Earth 9,10-Diborataanthracene Complexes Featuring Single-Molecule Magnet Characteristics. *Angew. Chem., Int. Ed.* **2024**, *63* (17), No. e202401372.

(35) Wernsdorfer, W.; Chakov, N. E.; Christou, G. Determination of the magnetic anisotropy axes of single-molecule magnets. *Phys. Rev. B* **2004**, *70*, 132413.

(36) (a) Pineda, E. M.; Lan, Y.; Fuhr, O.; Wernsdorfer, W.; Ruben, M. Exchange-bias quantum tunnelling in a CO_2-based Dy_4-single molecule magnet. *Chem. Sci.* **2017**, *8*, 1178−1185. (b) Hauser, A.; Münzfeld, L.; Schlittenhardt, S.; Uhlmann, C.; Leyen, L.; Moreno-Pineda, E.; Ruben, M.; Roesky, P. W. Cycloheptatrienyl-Bridged Triple-Decker Complexes. *J. Am. Chem. Soc.* **2024**, *146* (20), 13760−13769. (c) Moreno-Pineda, E.; Chilton, N. F.; Marx, R.; Dörfel, M.; Sells, D. O.; Neugebauer, P.; Jiang, S.-D.; Collison, D.; van Slageren, J.; McInnes, E. J. L.; Winpenny, R. E. P. Direct measurement of dysprosium(III)-dysprosium(III) interactions in a single-molecule magnet. *Nat. Commun.* **2014**, *5*, 5243. (d) Feng, D.-D.; Lu, F.; Liu, Z.-Y.; Wang, X.-G.; Li, X.-C.; Yang, E.-C.; Zhang, Y.-Q.; Zhao, X.-J. Side-Group Effect on the Slow Relaxations of {Dy2} Single-Molecule Magnets with Confined N2O6 Donors. *Inorg. Chem.* **2022**, *61*, 13133−13142. (e) Wang, H.-S.; Zhou, P.-F.; Wang, J.; Long, Q.-Q.; Hu, Z.; Chen, Y.; Li, J.; Song, Y.; Zhang, Y.-Q. Significantly Enhancing the Single-Molecule-Magnet Performance of a Dinuclear Dy(III) Complex by Utilizing an Asymmetric Auxiliary Organic Ligand. *Inorg. Chem.* **2021**, *60*, 18739−18752. (f) Long, J.; Habib, F.; Lin, P.-H.; Korobkov, I.; Enright, G.; Ungur, L.; Wernsdorfer, W.; Chibotaru, L. F.; Murugesu, M. Single-Molecule Magnet Behavior for an Antiferromagnetically Superexchange-Coupled Dinuclear Dysprosium(III) Complex. *J. Am. Chem. Soc.* **2011**, *133*, 5319−5328. (g) Chow, C. Y.; Bolvin, H.; Campbell, V. E.; Guillot, R.; Kampf, J. W.; Wernsdorfer, W.; Gendron, F.; Autschbach, J.; Pecoraro, V. L.; Mallah, T. Assessing the exchange coupling in binuclear lanthanide(iii) complexes and the slow relaxation of the magnetization in the antiferromagnetically coupled Dy2 derivative. *Chem. Sci.* **2015**, *6*, 4148−4159.

(37) Batista, L.; Paul, S.; Molina-Jirón, C.; Jaén, J. A.; Fensker, D.; Fuhr, O.; Ruben, M.; Wernsdorfer, W.; Moreno-Pineda, E. Magnetic behaviour of a spin-canted asymmetric lanthanide quinolate trimer. *Dalton Trans.* **2024**, *53*, 12927−12935.

(38) (a) Li Manni, G.; Fdez Galván, I.; Alavi, A.; Aleotti, F.; Aquilante, F.; Autschbach, J.; Avagliano, D.; Baiardi, A.; Bao, J. J.; Battaglia, S.; et al. The OpenMolcas Web: A Community-Driven Approach to Advancing Computational Chemistry. *J. Chem. Theory Comput.* **2023**, *19* (20), 6933−6991. (b) Ungur, L.; Chibotaru, L. F. Ab Initio Crystal Field for Lanthanides. *Chem.—Eur. J.* **2017**, *23* (15), 3708−3718. (c) Chibotaru, L. F.; Ungur, L. Ab initio calculation of anisotropic magnetic properties of complexes. I. Unique definition of pseudospin Hamiltonians and their derivation. *J. Chem. Phys.* **2012**, *137*, 064112. (d) Siegbahn, P. E. M.; Almlöf, J.; Heiberg, A.; Roos, B. O. The complete active space SCF (CASSCF) method in a Newton−Raphson formulation with application to the HNO molecule. *J. Chem. Phys.* **1981**, *74*, 2384−2396. (e) Roos, B. O.; Lindh, R.; Malmqvist, P.; Veryazov, V.; Widmark, P.-O. Main Group Atoms and Dimers Studied with a New Relativistic ANO Basis. *J. Phys. Chem. A* **2004**, *108* (15), 2851−2858. (f) Roos, B. O.; Lindh, R.; Malmqvist, P.; Veryazov, V.; Widmark, P.-O.; Borin, A. C. New Relativistic Atomic Natural Orbital Basis Sets for Lanthanide Atoms with Applications to the Ce Diatom and LuF_3. *J. Phys. Chem. A* **2008**, *112* (45), 11431−11435. (g) Widmark, P.-O.; Malmqvist, P.; Roos, B. O. Density matrix averaged atomic natural orbital (ANO) basis sets for correlated molecular wave functions. *Theor. Chim. Acta* **1990**, *77*, 291−306. (h) Malmqvist, P.; Roos, B. O.; Schimmelpfennig, B. The restricted active space (RAS) state interaction approach with spin−orbit coupling. *Chem. Phys. Lett.* **2002**, *357* (3−4), 230−240.

(39) Lines, M. E. Orbital Angular Momentum in the Theory of Paramagnetic Clusters. *J. Chem. Phys.* **1971**, *55*, 2977−2984.

(40) Chilton, N. F.; Anderson, R. P.; Turner, L. D.; Soncini, A.; Murray, K. S. PHI: A powerful new program for the analysis of anisotropic monomeric and exchange-coupled polynuclear d- and f-block complexes. *J. Comput. Chem.* **2013**, *34*, 1164−1175.

(41) Lunghi, A.; Totti, F.; Sessoli, R.; Sanvito, S. The role of anharmonic phonons in under-barrier spin relaxation of single molecule magnets. *Nat. Commun.* **2017**, *8*, 14620.
(42) (a) Han, T.; Ding, Y.-S.; Giansiracusa, M. J.; Chilton, N. F.; Winpenny, R. E. P.; Zheng, Y.-Z. Determinative Effect of Axial Linearity on Single-Molecule Magnet Performance in Dinuclear Dysprosium Complexes. *Chem.—Eur. J.* **2023**, *29* (29), No. e202300256. (b) Meng, Y.-S.; Xiong, J.; Yang, M.-W.; Qiao, Y.-S.; Zhong, Z.-Q.; Sun, H.-L.; Han, J.-B.; Liu, T.; Wang, B.-W.; Gao, S. Experimental Determination of Magnetic Anisotropy in Exchange-Bias Dysprosium Metallocene Single-Molecule Magnets. *Angew. Chem., Int. Ed.* **2020**, *59*, 13037−13043. (c) Ji, X.-Q.; Ma, F.; Xiong, J.; Yang, J.; Sun, H.-L.; Zhang, Y.-Q.; Gao, S. A rare chloride-bridged dysprosium chain with slow magnetic relaxation: a thermally activated mechanism via a second-excited state promoted by magnetic interactions. *Inorg. Chem. Front.* **2019**, *6*, 786−790. (d) Han, T.; Ding, Y.-S.; Li, Z.-H.; Yu, K.-X.; Zhai, Y.-Q.; Chilton, N. F.; Zheng, Y. Z. A dichlorido-bridged dinuclear Dy(iii) single-molecule magnet with an effective energy barrier larger than 600 K. *Chem. Commun.* **2019**, *55* (55), 7930−7933. (e) Tian, H.; Wang, B.-L.; Lu, J.; Liu, H.-T.; Su, J.; Li, D.; Dou, J. Consecutive one-/two-step relaxation transformations of single-molecule magnets via coupling dinuclear dysprosium compounds with chloride bridges. *Chem. Commun.* **2018**, *54*, 12105−12108.
(43) Taylor, M. D.; Carter, C. P. Preparation of anhydrous lanthanide halides, especially iodides. *J. Inorg. Nucl. Chem.* **1962**, *24*, 387−391.
(44) *Complexes of Bulky β-Diketiminate Ligands in Inorganic Syntheses*; Rauchfuss, T. B., Ed.; John Wiley & Sons, Inc.: Hoboken, 2010; Vol. *35*, pp 1−55.
(45) Sheldrick, G. M. A short history of SHELX. *Acta Crystallogr., Sect. A* **2008**, *64*, 112−122.
(46) *CrysAlisPro*, Agilent Technologies, 2014 Version 1.171.37.35 (release 13−08−2014 CrysAlis171.NET).
(47) Hübschle, C. B.; Sheldrick, G. M.; Dittrich, B. ShelXle: a Qt graphical user interface for SHELXL. *J. Appl. Crystallogr.* **2011**, *44*, 1281−1284.